280
7-25-77

2nd 9-26 H. 1258

COO/2616-2(Pt.2)

INVESTIGATION OF DIFFUSER-AUGMENTED WIND TURBINES PART II

Technical Report

R. A. Oman
K. M. Foreman
B. L. Gilbert

January 1977

Work Performed Under Contract No. EY-76-C-02-2616

Research Department
Grumman Aerospace Corporation
Bethpage, New York

ENERGY RESEARCH AND DEVELOPMENT ADMINISTRATION
Division of Solar Energy

DISCLAIMER

NOTICE

COO/2616-2(Pt.2)
Distribution Category UC-60

Grumman Research Department Report RE-534

INVESTIGATION OF DIFFUSER-AUGMENTED WIND TURBINES†

PART II — TECHNICAL REPORT

by

R. A. Oman
K. M. Foreman
B. L. Gilbert

January 1977

†This is a Final Report on Contract E(11-1)-2616 with U.S. Energy Research and Development Administration, Washington, D.C.

Prepared for

Wind Energy Conversion Branch
Division of Solar Energy

Research Department
Grumman Aerospace Corporation
Bethpage, New York 11714

Approved by: Charles E. Mack, Jr.
Charles E. Mack, Jr.
Director of Research

ACKNOWLEDGMENT

The authors gratefully acknowledge the contribution of Mr. J. Crouzet-Pascal in calculating the structural design of the baseline diffuser configuration presented in this report. The potential flow calculations for the conical diffuser were performed by Dr. A. Loeffler and Mr. D. Vanderbilt. Details of these investigations beyond those contained in this report may be obtained by request to the Grumman Research Department. Also we thank Harvey Jordan and George Homfeld for their assistance in the model fabrication.

THIS PAGE

WAS INTENTIONALLY

LEFT BLANK

TABLE OF CONTENTS

LIST OF ILLUSTRATIONS

1. INTRODUCTION

This contract was awarded to allow the concept of a Diffuser-Augmented Wind Turbine (DAWT) in its effective modern form to be evaluated against more conventional wind turbine concepts. There are several aspects of modern technology that offer significantly greater advantages to these shrouded systems than had been realized in past evaluations. The most important of these are:

1. The promise of modern boundary layer control to reduce the surface area (i.e., length) requirements of an efficient diffuser by an order of magnitude

2. The realization (since confirmed by experiment) that an extremely beneficial augmentation of a shrouded wind turbine results from the effects of turbulent momentum exchanges between the turbine/diffuser wake and the accelerated peripheral flow. This momentum exchange results in a greatly reduced exit plane pressure that has been as beneficial as the effect of the diffuser itself.

3. The promise of synergistic advantages derived from design features that are naturally compatible with the diffuser/shroud system; e.g., an upstream stator that inexpensively replaces the rotor pitch change mechanism and the electrical frequency/phase matching equipment, and a three-point suspension system that may significantly reduce tower and structural costs.

4. An increasing concern for the cost and development risk associated with very large rotors, leading to

significant advantages for a system that produces larger rated power from a rotor that is limited in size by aeroelastic design constraints

The overriding criterion for the evaluation of interim and final configurations is the cost of the energy they would produce in production quantities. This is reflected primarily in the capital cost comparison for competing concepts, with minor influences from other cost factors such as operating wind range, esthetics, and maintenance requirements. Cost estimates for components of both the DAWT and conventional systems in production quantities are, unfortunately, highly speculative at this time; but we have tried to use the best cost data we can get and to use estimating methods that are easily adjusted for changes in cost data. Cost and practicality projections are the major factors that determined the choices and sequence of the configurations we have tested and analyzed, and we expect to continue that policy.

Our program was summarized in Ref. 1. It closely parallels the work of Igra (Ref. 2). Although independently derived, most of our decisions as to possibilities and relative promise of different approaches have turned out to be very similar to his. Apart from this general confirmation of views and useful exchanges of information, Igra's work has been of central importance to our program in that it offered the first direct experimental evidence of very large (favorable) exit plane pressure reductions. This enabled us to project with some assurance the large augmentation ratios that were the early analytical results of our work, and are now substantiated by our own experiments. Without Igra's data at an early stage in the concept there would have been no defensible basis for expecting such a large beneficial effect from downstream interactions.

In our interim report, the tentative conclusions presented were derived principally from cursory surveys designed to uncover qualitative trends quickly. The essence of these conclusions remains unchanged after one year of work, except for some minor detail. What has changed significantly is the precision of our measurements, the understanding and insight into the fluid mechanics, and the specifics of performance details that lead to clearer and more meaningful economic analyses. The more complete experimental investigations, more exhaustive theoretical analyses, and better quality of economic data associated with this annual report have improved further the over-all virtues of the DAWT concept over what had previously been reported.

2. DEVELOPMENT OF EFFICIENT, COMPACT DIFFUSERS

An increase in the energy available to a wind turbine rotor of fixed size is possible by installing it at the entrance to a diffuser. As the cross sectional area of the diffuser duct increases downstream of the turbine, continuity of mass requires a decrease in the axial velocity, producing a corresponding increase in pressure. Therefore, the inlet to the diffuser is at a significantly lower pressure than that at its exit. When placed at the exit of a turbine, the diffuser will substantially increase the mass flow and total pressure drop across the turbine. The power available to the turbine is proportional to this product.

The diffuser design must have the smallest possible structural cost, while still maintaining an appreciable subatmospheric pressure at the turbine exit plane and a large pressure recovery within the diffuser. This requires diffusers that are reliably free of extensive flow separation, that maintain effective performance characteristics, but possess divergence half angles much greater than the conventional 3 to 6°. A solution to boundary layer separation in very strong adverse pressure gradients becomes the heart of the problem.

Several design concepts were examined, of which the two most promising were studied. One concept employs the tangential injection of high energy air available from the external wind. The additional momentum supplied to the boundary layer fluid helps it flow against the severe adverse pressure gradient and overcome the frictional losses that are present in the wall region. This, if properly done, has the effect of preventing flow separation from the wall (the primary cause of failure of large angle diffusers). The other concept employs a diffuser/ejector made from

one or more short ring airfoils. Each ring airfoil produces a al aerodynamic pressure distribution along the internal ring surface and induces more flow through the turbine. Further augmentation may be obtained by the use of series of rings or by the addition of flaps. These designs combine the advantages of good structural efficiency, low surface area, boundary layer control, and high turning capacity.

In the following subsections, we include several mathematical analyses that were developed to guide the experiments. The first of these explains the interaction of the various components of a DAWT showing the effect on over-all performance of the performance parameters of each component. The experimental apparatus is then briefly described. Next, the method of simulating a turbine by use of calibrated screens is discussed. Another analysis then attempts to indicate the amount of boundary layer blowing that is required to overcome wall friction and thereby maintain the boundary layer at the same axial momentum level as inviscid flow in a diffuser. Next, the experimental program on boundary layer controlled diffusers is described, and the most useful results summarized. A description of the design and testing of our ring wing configurations follows. This section concludes with a brief discussion of the origin and significance of the observed exit plane pressure reductions.

ANALYSIS OF THE DIFFUSER-AUGMENTED WIND TURBINE

The following brief presentation outlines a simple one dimensional optimization of the DAWT. Priorities in our experimental work were established by consideration of the effects of the critical performance parameters that are given below, coupled with the cost associated with achieving better component performance in oduction installations.

Referring to Fig. 1 for notation, the ideal power available is given by the product of the total pressure extracted by the turbine and the volumetric flow rate

$$\mathcal{P}_i = \Delta H_{23}(V_2 A_2) \tag{1}$$

Normalizing by the total available free wind power (kinetic energy times flow rate) in a streamtube of area A_2 gives an ideal power coefficient

$$C_{\mathcal{P}_i} = \Delta H_{23}(V_2 A_2)/(\tfrac{1}{2}\rho V_o^2)(V_o A_2) \tag{2}$$

From Bernoulli's theorem, the total pressure is

$$P_t = p_o + \tfrac{1}{2}\rho V_o^2 = \Delta H_{14} + p_4 + \tfrac{1}{2}\rho V_4^2 \tag{3}$$

The following definitions have been applied:

The total loss between the duct inlet (Station 1) and the exit (Station 4) is

$$\Delta H_{14} = \Delta H_{23} + \tfrac{1}{2}\rho[K_i V_o^2 + (1 - \eta_D)(V_3^2 - V_4^2)]$$

$$K_i = \text{inlet loss coefficient} = -(p_2 - p_1)/\tfrac{1}{2}\rho V_o^2 \tag{4}$$

$$\eta_D = \text{diffuser efficiency} = (p_4 - p_3)/\tfrac{1}{2}\rho(V_3^2 - V_4^2)$$

and from flow continuity

$$V_1 = V_2 = V_3$$

$$V_3 A_3 = V_4 A_4$$

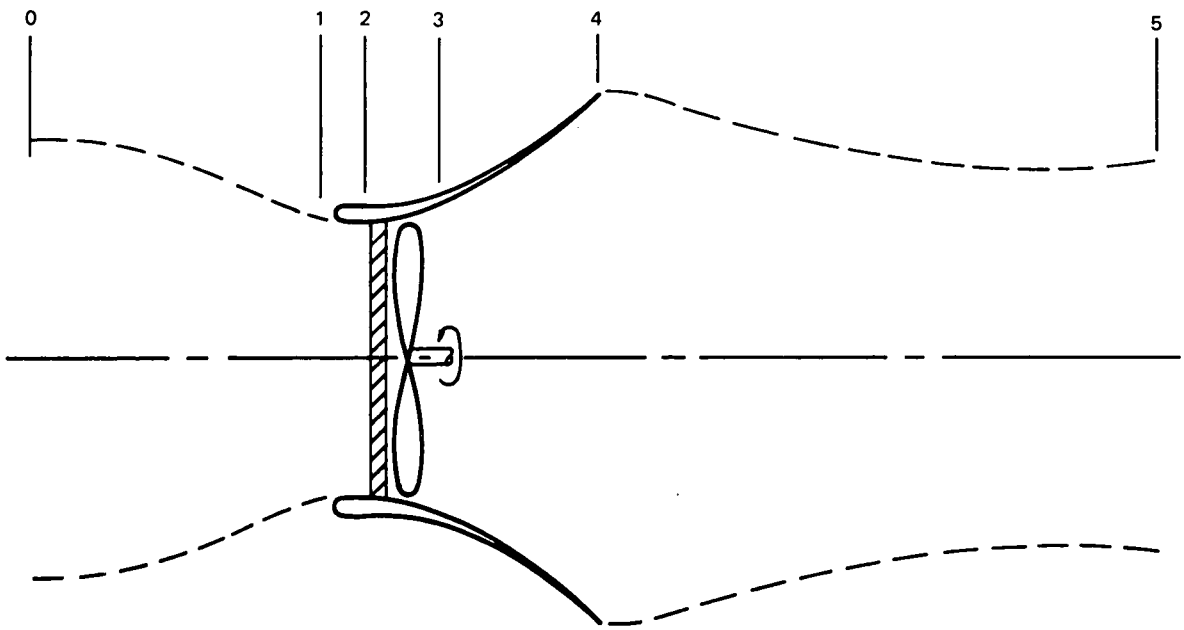

Figure 1 Schematic of Diffuser-Augmented Wind Turbine (DAWT) Showing Reference Stations

Introducing three nondimensional parameters

$$\epsilon = V_2/V_o \quad , \quad \lambda = A_3/A_4$$

and

$$C_{p_4} = (p_4 - p_o)/\tfrac{1}{2}\rho V_o$$

into Eqs. (3) and (4) and normalizing by $\tfrac{1}{2}\rho V_o^2$ gives

$$\frac{\Delta H_{23}}{\tfrac{1}{2}\rho V_o^2} = \left(1 - K_i - C_{p_4}\right) - (1 - \eta_D)\epsilon^2 - \eta_D \epsilon^2 \lambda^2 \qquad (5)$$

Substituting Eq. (5) into Eq. (2) gives the power coefficient

$$C_{\mathcal{P}_i} = \epsilon \frac{\Delta H_{23}}{\tfrac{1}{2}\rho V_o^2} = \left(1 - K_i - C_{p_4}\right)\epsilon - \left(1 - \eta_D(1 - \lambda^2)\right)\epsilon^2 \qquad (6)$$

Equation (5) defines the pressure difference that prevails across the turbine station for a particular velocity ratio ϵ. If a stator precedes the turbine, ΔH_{23} will be apportioned between stator and rotor, in which case only the pressure drop across the rotor can contribute to the shaft power. The main significance of Eq. (6) is that the power available to a perfect ducted turbine can be made to increase significantly by a small rotor/exit area ratio, a high diffuser efficiency (η_D), an optimum disk velocity ratio (ϵ), and a strongly negative base pressure coefficient (C_{p_4}). The velocity ratio will be determined by the disk loading $(\Delta H_{23}/\tfrac{1}{2}\rho V_o^2)$ of the turbine that is installed in the duct, which is where the detailed design of the turbine begins.

There is a particular value of ϵ, and disk loading $\Delta H_{23}/\tfrac{1}{2}\rho V_o^2$ that results in maximum $C_{\mathcal{P}_i}$, that is obtained by conventional optimization

$$\epsilon_{opt} = \sqrt{\frac{1 - K_i - C_{p_4}}{3(1 - \eta_D + \lambda^2 \eta_D)}} \tag{7}$$

$$C_{T_o} = \left(\frac{\Delta H_{23}}{\frac{1}{2}\rho V_o^2}\right)_{opt} = \frac{2}{3}\left[1 - K_i - C_{p_4}\right] \tag{8}$$

The maximum power available to a stator-turbine configuration is that given by substituting ϵ_{opt} into Eq. (6) and multiplying by the fraction of ΔH_{23} that prevails across the rotor.

Equations (6) through (8) indicate the key issues in a DAWT. First, there is an "infinite area ratio limit" as $\lambda \to 0$, for which ϵ and C_{P_i} are asymptotic. Secondly, we can see that inlet losses detract but exit plane suction augments the power coefficient directly insofar as they are significant compared to unity. Note that C_{p_4} is a negative value representing an exit plane suction. Thirdly, the diffuser efficiency is less important to over-all performance as area ratio decreases ($\lambda \to 1$). Most important of all, increased power coefficients will result from increasing the turbine velocity ratio ϵ, although losses in the diffuser will become more significant at higher values of ϵ. For typical values of the DAWT, we may use $K_i = 0$, $C_{p_4} = -0.5$, $\eta_D = 0.85$, and $\lambda = 0.33$. This set produces $\epsilon_{opt} = 1.43$, $(\Delta H_{23}/q_o)_{opt} \approx 1$, and $(C_{P_i})_{opt} = 1.43$. Contrasting these values with those obtained from the conventional wind turbine where $\epsilon_{opt} = 0.67$, $(\Delta H_{23}/q_o) = 8/9$, and $(C_{P_i})_{opt} = 0.593$, gives a computed optimum diffuser augmentation ratio $r = (C_{P_i})_{DAWT} / (C_{P_i})_{CWECS} = 2.41$. As an additional benefit, the velocity entering the disk of the DAWT would be 2.13 times that for the conventional wind turbine, which has great significance for large practical designs in that the turbine can operate at lower wind velocities.

EXPERIMENTAL TECHNIQUES

Apparatus

The experiments were conducted in a low speed, low turbulence level, free jet tunnel facility (see Fig. 2). The core region of a free jet flow was used as the test section in which uniform wind conditions were simulated. The 29.2 cm circular jet issued from a 91.4 x 91.4 cm settling chamber via a standard ASME long radius nozzle. The mean flow was uniform across the exit and did not appear to possess the characteristic acceleration usually found at the periphery of jets. The maximum velocity of the facility was 17.7 meters/sec (58 fps), however, velocities of about 13.0 meters/sec (43 fps) were used for the tests reported here. The use of blockage models in this facility indicated that the relatively free stream disturbance was much less than the equivalent disturbance for a closed wind tunnel with the same relationship of model to test section area size.

The models were supported in the core region of the jet by 1.6 mm (1/16 in.) diameter brass rods. These rods were supported by three 9.5 mm (3/8 in.) diameter threaded rods that were cantilevered from a collar at the nozzle exit. The air flow accelerating due to an exit plane blockage and nozzle contraction would contribute

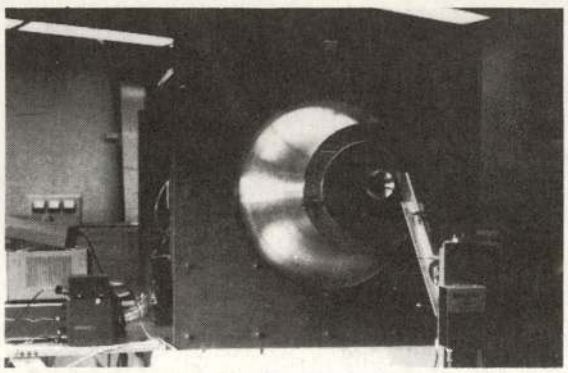

Figure 2 Jet Tunnel With DAWT Model Installed

an apparent improvement in the induced velocity into the model. Therefore, models were maintained in the core region but well downstream of the jet exit plane.

The boundary layer controlled diffusers were originally constructed from 0.009 in. stainless steel shim stock, rolled into appropriate shapes, and soft soldered. Later models, requiring greater precision in construction, were spun from 0.030 in. soft aluminum over suitable mandrils. The required sections were then lathe cut from master blanks. Slot spacings were maintained by shimming the diffuser sections with the appropriately sized bell wire spacers. For the ring wing models, a template of the aerodynamic cross section was hand cut. The finished models were machined on a tracer lathe. Uniform screens of various solidities were mounted inside or on the front of a supporting ring that were used in the models to simulate turbines. These rings were usually supported inside the model by 0.025 in. stainless steel pins. Connections between the various components were made by solder or epoxy cement.

Figure 3 shows two photographs of BLC diffusers. The first photo shows three diffusers: 20, 30, and 40°, with the same exit to turbine disk ratio (2.78) and inlet slot size. The 20° diffuser is of earlier construction employing rolled stainless steel sheet and the other two are spun aluminum. The decrease in material from 20 to 40° is obvious. The second photograph is a three-quarters view of the 30° diffuser showing the mounting details of the screen ring, inlet, and auxiliary slots. The screen is 14 mesh/in. with a screen pressure drop of about 0.37 q_2.

The first photograph in Fig. 4 is a William's contour ring wing diffuser with an airfoil shaped contour flap. The turbine simulator screen is not installed. The second photograph is of a NACA 4412 airfoil wing ring with 20 percent chord split plate

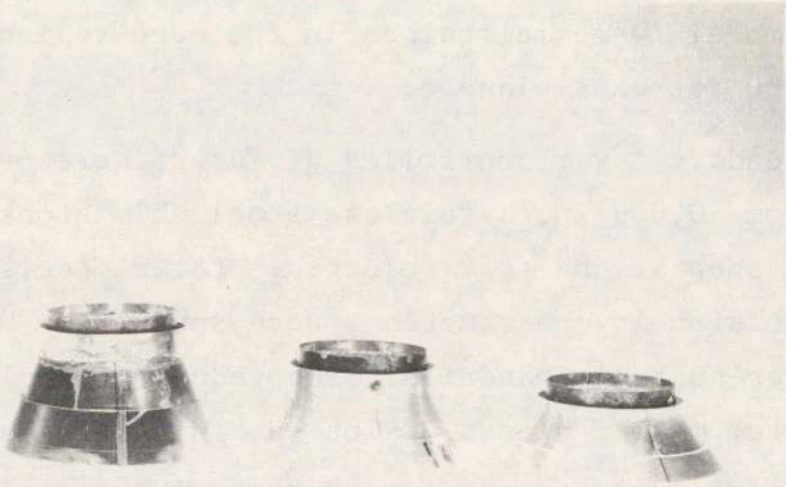

a) (left to right) 20°, 30°, and 40° half angle models each with an area ratio of 2.78

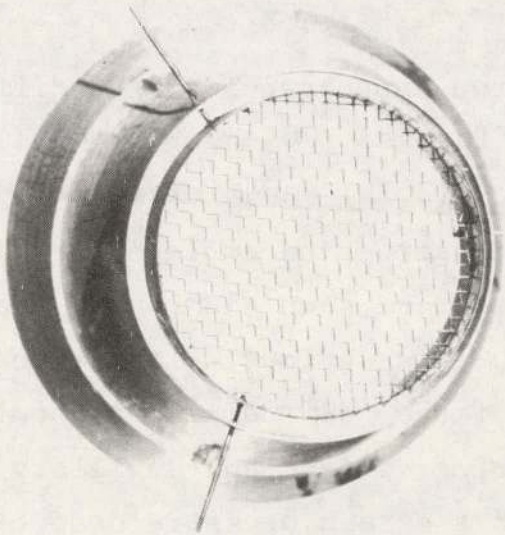

b) baseline configuration; 30° diffuser with an area ratio of 2.78 (screen installed $C_T = 0.37$)

Figure 3 Boundary Layer Controlled (BLC) Diffuser Models

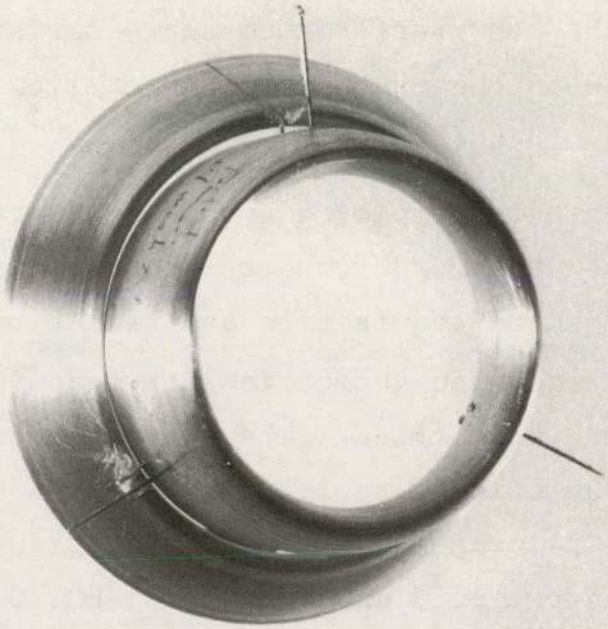

a) Williams "A" with airfoil flap

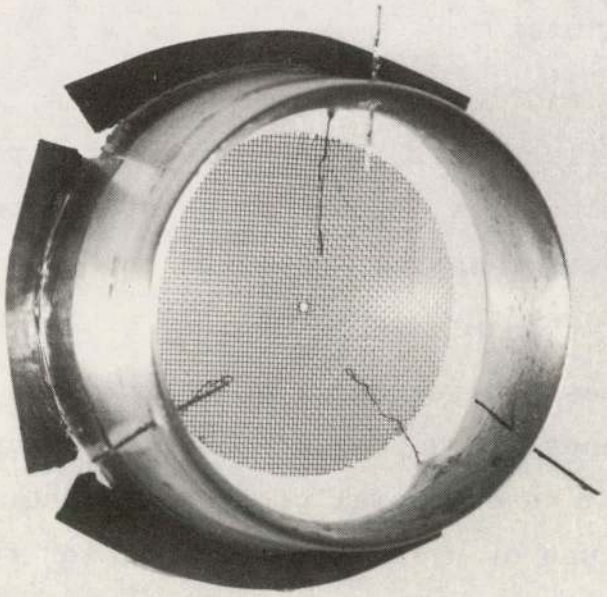

b) NACA 4412 with split flap (screen installed $C_T = 0.64$)

Figure 4 Two Ring Wing Diffuser Configurations

flaps. These flaps were constructed of lead tape. The screen is mounted downstream of the minimum diameter section at a position which exhibited the best performance characteristics. The deformation of the screen at the centerline is to allow the instrumentation probe to pass through the screen.

The instrumentation employed a transconductance differential pressure transducer that was found to be an expedient experimental technique for both data acquisition and reduction. An assortment of various probe sizes and geometries for measuring total, dynamic, and static pressure were tried. The most successful arrangement utilized a single static pressure probe mounted with its pressure ports in the same plane as a single total pressure probe. These were constructed from 1.27 mm (0.05 in.) OD, 0.2 mm (0.008 in.) wall stainless steel tubing that would readily pass through the 6.3 mesh/cm screen size used in many of the experiments. Screens with smaller mesh spacings required small deformations at axial survey positions. Complete axial static and total pressure surveys were taken from an upstream to a downstream position passing right through the turbine simulator.

For the axial and radial pressure measurements, the probes were mounted on a tridirectional, motor-driven traversing mechanism. This device gives an electrical output proportional to its position so that the pressure versus spatial position could be directly recorded by an x-y pen recorder.

In general, only centerline axial and exit plane radial surveys were made. In some cases, more complete determinations were made by taking axial surveys at seven radial positions. The measurements were augmented by the use of nylon threads used for flow visualization.

Turbine Simulation

Since a family of wind turbines is impractical to build for an exploratory investigation of small scale diffuser models, we have

simulated the turbine energy extraction by screens that dissipate e energy at the turbine station. We represent the turbine performance by the local disk loading coefficient

$$C_T = (p_2 - p_3)/\tfrac{1}{2}\,\rho V_2^2 \qquad (9)$$

The power extracted per unit area is the product of the total pressure drop and the local velocity.

For uniform wire screens, the total pressure drop for flow normal to the screen, Δp, is related to dynamic pressure immediately upstream of the screen $\tfrac{1}{2}\,\rho V_2^2$, by a coefficient, K_t, where

$$K_t = \Delta p/\tfrac{1}{2}\,\rho V_2^2 \qquad (10)$$

For rectangular mesh screens the coefficient is a function of Reynolds number, porosity ratio, and screen geometric projected area. We define the porosity ratio, $a = [1 - (d/\ell_1)] \cdot [1 - (d/\ell_2)]$, where d = wire diameter and ℓ_1 and ℓ_2 are the distances between wires in the two principal directions. For a square mesh arrangement $\ell_1 = \ell_2 = \ell$ so $a = [1 - d/\ell]^2$, and the solidity, $b = (1 - a)$. For uniform screening, the Reynolds number is based on wire diameter. For a local wind speed of about 15 meters/sec (50 foot/sec), corresponding to our expected experimental conditions, the Reynolds number $(= Vd/\nu)$ is about 240 for 0.229 mm (0.009 in.) diameter wire.

Several theoretical relations (described in Ref. 3) and one engineering design method (Ref. 4) were examined to calculate the resistance coefficient, K_t. However, since our actual screen installations can include other drag elements, such as support rings, rods, and small globs of epoxy cement or solder, as well as the screens, we have preferred to measure the total pressure loss in :u during a diffuser model test. As might be expected, the total simulator assembly usually exhibited a slightly higher K_t than any predictive or measured value for the screen alone.

Data Reduction

The ideal power coefficient is given in Eq. (2). This expression may be normalized by the optimum power derived from an ideal turbine, 0.593, to define an augmentation ratio

$$r = \frac{\Delta H V_2}{\frac{1}{2} \rho V_o^2 V_o (0.593)} \tag{11}$$

where ΔH is the total pressure drop across the turbine (screen) = $p_2 - p_3$. The magnitude of ΔH is a function of the particular screen used and the local dynamic pressure. Expressing this relationship as $\Delta H = K_s q_2$ where the value of K_s is measured directly in the system, Eq. (11) becomes

$$r = \frac{K_s}{0.593} \left(\frac{q_2}{q_o}\right)^{3/2} \tag{12}$$

Figure 5 shows the standard measurements used to determine the system augmentation. The dynamic pressure q_2 is given as $\Delta q_{inlet} + q_o$. The screen factor is computed as $-\Delta H/q_2$. Measurements of static, dynamic, and total pressure were usually made.

Complete axial surveys at different radial locations were not made in all cases. As can be seen in Fig. 6, there exists in all cases an increasingly greater induced local flow rate with increase in radius. The greatest induced flow is near the outer edge of the simulated turbine. This corresponds to a greater augmentation at positions where there is larger annular area and higher turbine blade speeds; that is, where it is more beneficial. Further, the poorest performance is at the centerline where a real turbine will have a centerbody and therefore no power extraction. We attribute this effect to the inlet flow field, and to the ejector effect of the peripheral slot.

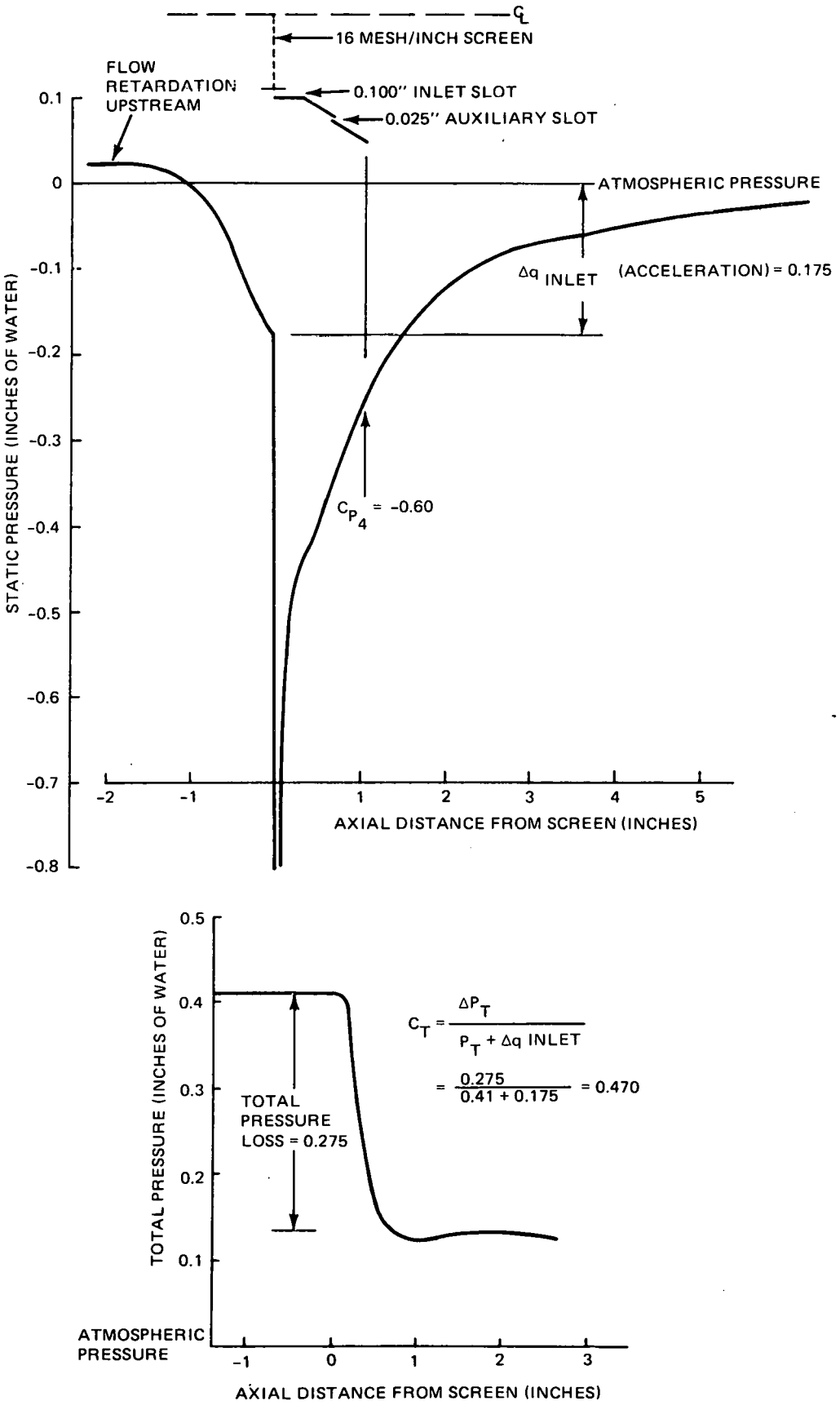

igure 5 Typical Centerline Axial Static and Total Pressure Surveys in the 30° Half-Angle Diffuser Shown, C_T = 0.47

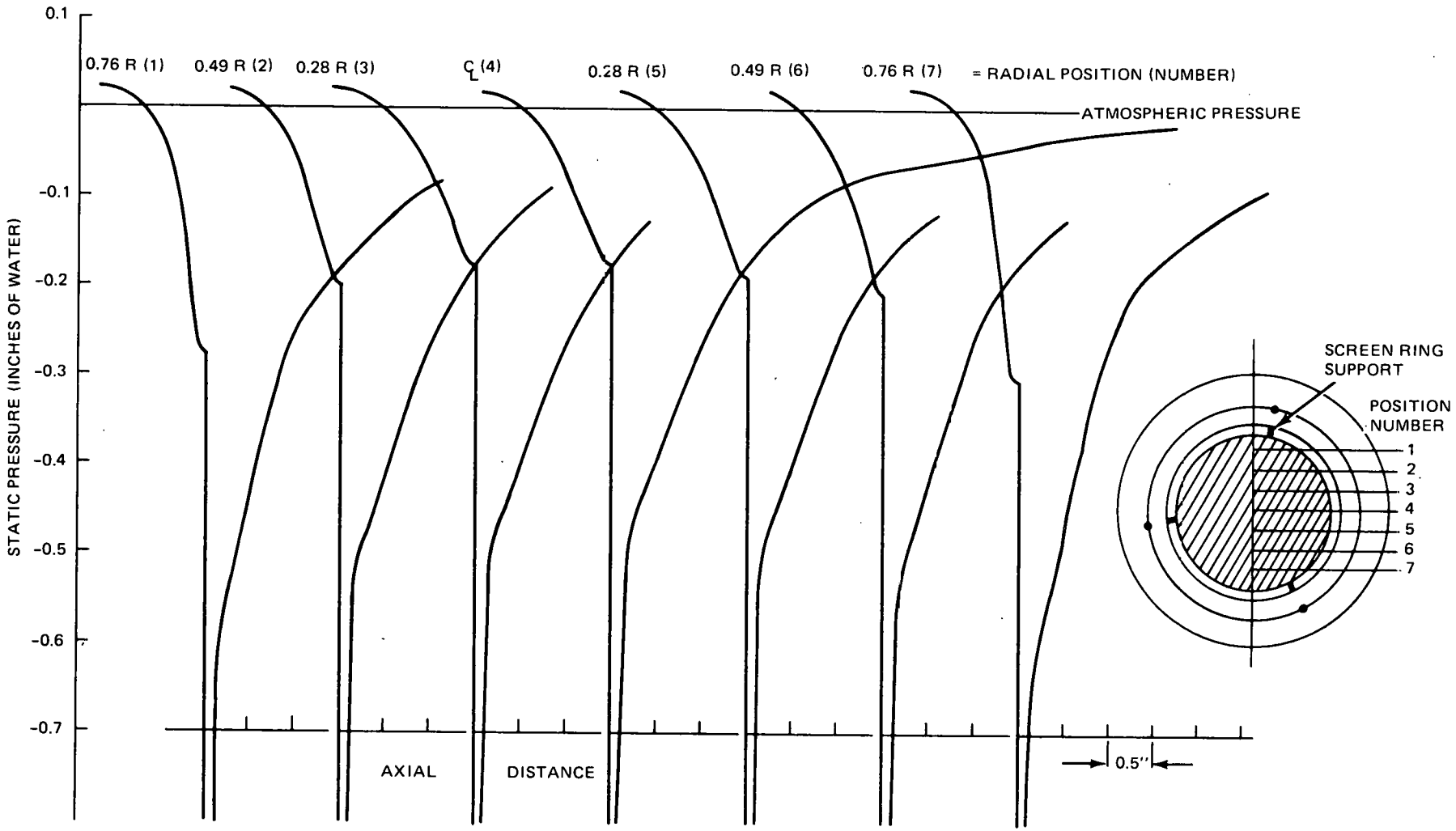

Figure 6 Axial Static Pressure Surveys at Various Radial Positions in a 30° Baseline Diffuser (Abscissas Displaced for Clarity)

The local screen pressure drop has a strong radial dependence a consequence of a constant value of K_s and the increased q_2. The screen simulator was generally mounted on the front of, or in the middle of, a stainless steel ring shroud. With the screen mounted at the leading edge of the shroud, the local static pressure drop increased substantially with radius, while the dynamic pressure had a much smaller percentage increase. A similar test, with the screen mounted in the middle of the shroud, showed a substantial variation in inlet velocity but a much smaller variation in total pressure loss, consistent with a uniform screen loss coefficient. When no shroud was used, the screen pressure drop fell rapidly toward the (now) poorly defined outer edge.

The anomalous behavior of the forward mounted shrouded screen, where the pressure drop apparently increased without a corresponding increase in local inlet velocity and the ambiguous outer edge of an unshrouded screen lead to the use of the center-mounted screen geometry. The geometry had an inlet section to the screen and a constant diameter exit section. This assured that the approximation of constant duct area across the turbine station was well simulated.

When only the centerline pressure survey was conducted, the augmentation was computed on the basis of the centerline acceleration used in Eq. (12) and denoted as $r_{\text{¢}}$. For cases where the axial surveys were conducted at several radial locations, an average augmentation, $\bar{r}$, was found. The local induced velocity profile was curve fit with a polynomial and the average augmentation was computed by integration over the disk area. No correction for the presence of a centerbody was applied. In addition, the radial location where the average velocity was found, the addition augmentation over the centerline determination, and diffuser efficiency or alternatively, an effective area ratio, were also computed.

In almost all cases, the radius corresponding to average augmentation was 75 percent of the outer turbine radius. In the boundary layer controlled diffusers, the average augmentation exceeded the centerline determination by about 22 percent in the 20°, 37 percent in the 30°, and 42 percent in the 40° diffusers for a disk loading of 47 percent. These generalizing numbers were a function of disk loading, indicating that the lower the loading, the more severe the velocity profile distortion. For the ring wings, the average differed from the centerline augmentation by about 18 percent, implying a much more uniform inlet velocity profile. These results are summarized in Fig. 7 Curves are drawn

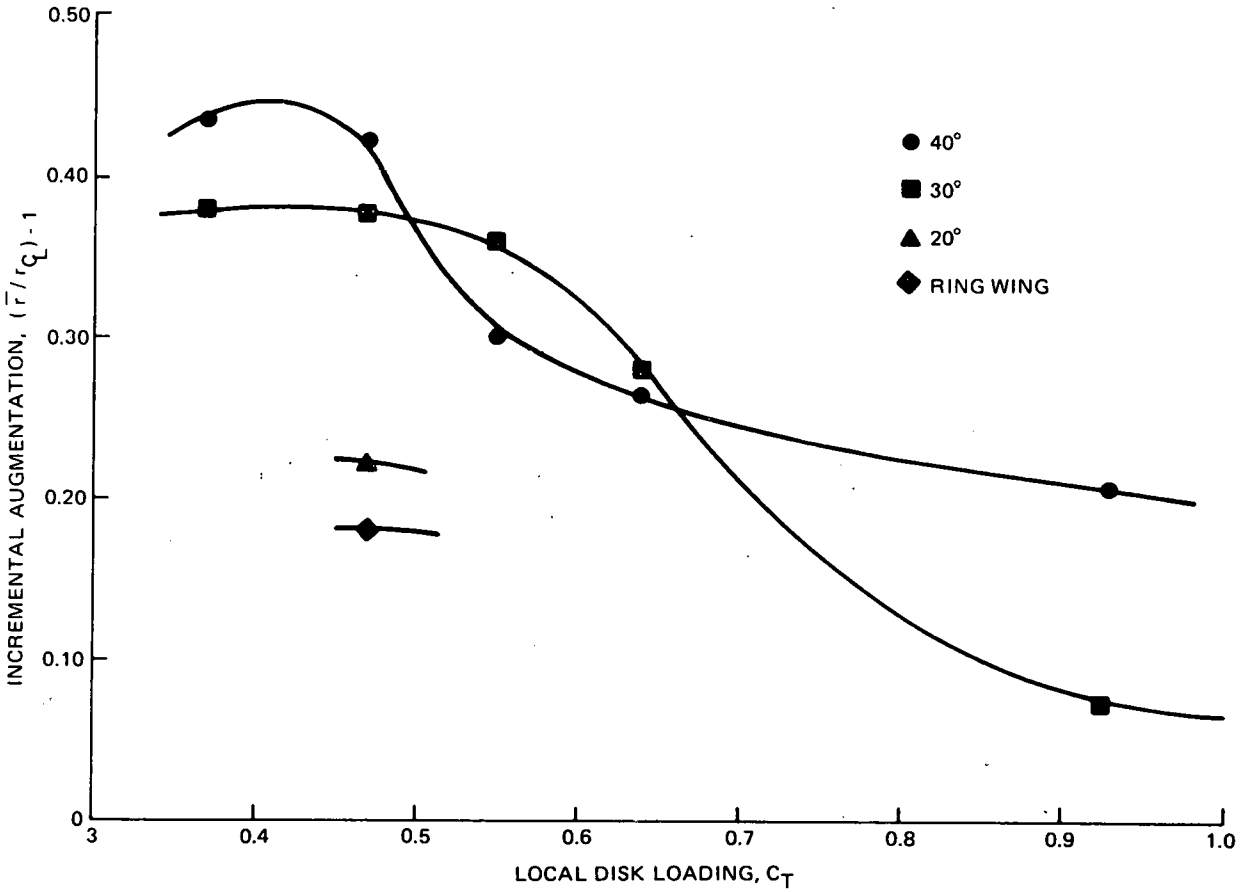

Figure 7 Incremental Improvement of Mass-Averaged Augmentation Ratio Over the Centerline Value

through the experimental data to indicate trends. Unless indicated ıerwise, all curves presented in this report serve this purpose.

In general, axial profile information was supplemented by radial surveys. These usually measured static, dynamic, and total pressure. Qualitative measurements were made using nylon thread singly, on a rake, or attached to the diffuser wall.

BOUNDARY LAYER CONTROLLED DIFFUSER

Theoretical Analysis

A mathematical analysis of the boundary layer controlled diffuser (shown in Fig. 8) was conducted assuming a simplified one dimensional model. This analysis is useful for estimating the amount of injected fluid required to prevent separation and the effect of injection on pressure recovery. An important concern that

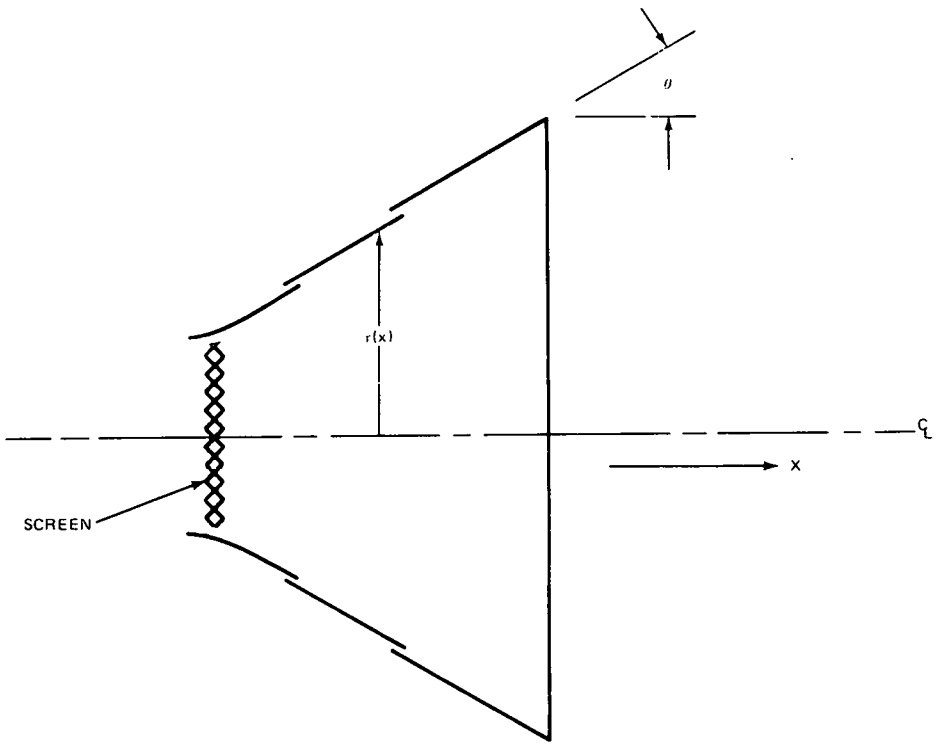

Figure 8 Sketch of a Typical Boundary Layer Controlled Diffuser Model

has to be considered theoretically is the detailed process of injection of high energy fluid through discrete slots. This aspect of the boundary layer control phenomenon must be properly understood so that the process may be scaled confidently to a full size prototype. We hope to make a significant contribution to that problem in the second year's effort.

In this analysis, besides considering the flow to be one dimensional, a uniform porosity fraction is assumed. The details of slot mechanics and the flow through the turbine have been modeled by empirical loss coefficients used in a modified Bernoulli's equation. Then, based upon a chosen skin friction criterion, the analysis predicts the fractional perturbation of the pressure gradient in a modeled diffuser relative to an ideal frictionless flow in a diffuser of the same divergence. The entire boundary layer control concept is designed to inhibit flow separation caused by friction. The frictionless diffuser is the ideal situation, so it is a useful reference condition from which to evaluate the effect of injection on pressure recovery.

The skin friction is assumed to be dominated by the injected fluid, therefore is characterized by the injection velocity and a skin friction coefficient typical of turbulent boundary layers in zero pressure gradient. The amount of injected fluid is controlled by the designer's choice of the porosity, i.e., slot area per unit wall area. The goal of slot injection is to cancel the wall friction so the flow acts reversibly. Accordingly, the required injected momentum will be some multiple of the expected shear stress, and we expect that multiple to be near unity. The analysis will predict the perturbation of the pressure gradient that results from injection of different skin friction multiples.

In a one dimensional diffuser of local radius $r(x)$ and divergence half-angle θ, let the local velocity be $u(x)$ and let mass enter continuously through the wall at a local (axial) velocity of $v(x)$. The local porosity fraction is $h(x)$. The equation of mass conservation in steady flow is

$$\rho u \pi r^2 + \rho v \pi (2r + dr) h ds = \rho (u + du) \pi (r + dr)^2 \qquad (13)$$

where $ds = dx \sec \theta$.

Simplifying and taking the limit, we get

$$hv \sec \theta = u \tan \theta + \frac{r}{2} \frac{du}{dx} \qquad (14)$$

The conservation of axial momentum is satisfied by balancing pressure forces, the shear stress, τ, on the walls, and the net momentum flux through an infinitesimal element, giving

$$- \frac{dp}{dx} = \frac{2\tau}{r} + \frac{2\rho}{r} \left\{ u^2 \tan \theta - v^2 h \right\} + 2\rho u \frac{du}{dx} \qquad (15)$$

with boundary conditions $u = u_3$, and $r = r_3$ at $x = 0$, the exit of the turbine.

Equations (14) and (15) may be combined to give

$$- \frac{dp}{dx} = \frac{2\tau}{r} + \frac{2\rho}{r} [hv(2 u \sec \theta - v) - u^2 \tan \theta] \qquad (16)$$

where $r = r_3 + x \tan \theta$.

The flow through the wall slots is determined by the difference between the external total pressure and the local internal static pressure

$$p_o + \tfrac{1}{2} \rho u_o^2 = p(x) + (1 + K_s) \tfrac{1}{2} \rho [v(x)]^2 \qquad (17)$$

where K_s is the slot loss coefficient $= \Delta p_s / \tfrac{1}{2} \rho [v(x)]^2$.

Similarly, the flow through the turbine can be described by using the turbine disk loading coefficient, K_t

$$p_o + \tfrac{1}{2}\rho u_o^2 = p_3 + (1 + K_t)\tfrac{1}{2}\rho u_3^2 \tag{18}$$

where K_t is based on local velocity and $u_2 = u_3$

The core flow inside the diffuser will appear approximately frictionless so

$$p_3 + \tfrac{1}{2}\rho u_3^2 = p(x) + \tfrac{1}{2}\rho[u(x)]^2 \tag{19}$$

combining Eq. (17) through Eq. (19) gives

$$(1 + K_s)\tfrac{1}{2}\rho v^2 = K_t(\tfrac{1}{2}\rho u_3^2) + \tfrac{1}{2}\rho u^2$$

or rearranging

$$v^2 = (K_t u_3^2 + u^2)/(1 + K_s) \tag{20}$$

Dividing by u^2 and noting that as a first approximation, the injected mass flow effect is small,† the approximate continuity condition

$$\left(\frac{u_3}{u}\right) = \left(\frac{r}{r_3}\right)^2$$

may be applied to give

$$\left(\frac{v}{u}\right)^2 = \left[K_t\left(\frac{r}{r_3}\right)^4 + 1\right] \Big/ (1 + K_s) \tag{21}$$

The perturbation of the pressure gradient due to friction and injected secondary fluid may be calculated by noting that the pressure gradient in an ideal diffuser of the same angle is given by

†Note that this assumption puts an upper limit on v in Eq. (21), which slightly exaggerates the estimate of pressure gradient perturbation.

$$\left(\frac{dp}{dx}\right)_o = - \rho u \frac{du}{dx}$$

ich is driven solely by the change in diffuser area, when this is combined with continuity

$$\frac{du}{dx} = - \frac{2u}{r} \tan \theta$$

yields

$$\left(\frac{dp}{dx}\right)_o = 2\rho u^2 \tan \theta / r \qquad (22)$$

Subtracting Eqs. (22) from Eq. (16) gives

$$\Delta \equiv \frac{dp}{dx} - \left(\frac{dp}{dx}\right)_o = - \frac{2}{r} \left(\tau + h(2 \rho uv \sec \theta - \rho v^2)\right) \qquad (23)$$

Assume that the shear stress is dominated by the injected fluid, so that

$$\tau = C_f(\tfrac{1}{2} \rho v^2) \qquad (24)$$

A solution to Eq. (23) is possible by choosing an injection criterion. A physically reasonable selection is that the additional momentum supplied by the secondary fluid is equal to some multiple of the frictional loss

$$\rho h v^2 = \alpha \tau \qquad (25)$$

In Eq. (23), Eq. (25) gives

$$\Delta = - \frac{2}{r} h\left(\left(\frac{1 - \alpha}{\alpha}\right)\rho v^2 + 2 \rho uv \sec \theta\right) \qquad (26)$$

and the fractional change is

$$\xi = \frac{\Delta}{\left(\frac{dp}{dx}\right)_o} = h\left[\frac{\left(\frac{\alpha - 1}{\alpha}\right)\left(\frac{v}{u}\right)^2}{\tan \theta} - \frac{2\left(\frac{v}{u}\right)}{\sin \theta}\right] \qquad (27)$$

where from Eqs. (24) and (25)

$$\alpha C_f \tfrac{1}{2} \rho v^2 = h \rho v^2$$
$$h = \alpha C_f / 2 \qquad (28)$$

and (v/u) is given by Eq. (21) as a function of x. It is desirable that ξ be a small number so that pressure recovery is maximized. For parametric values of the selected coefficient α, the fractional pressure gradient perturbation is shown on Fig. 9.

Since the turbulent skin friction coefficient can range from 0.001 to 0.01, the above indicates that a very small wall porosity should exist to prevent separation, and that these small porosities produce small changes from the ideal pressure gradient that would exist in a frictionless diffuser with solid walls.

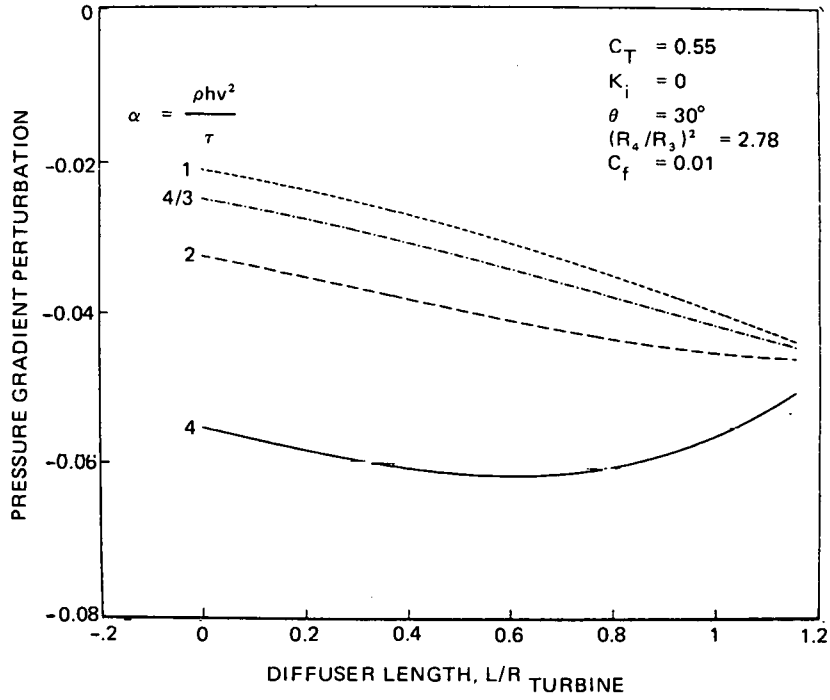

Figure 9 Pressure Gradient Change From an Ideal Diffuser for Various Amounts of Injected Secondary Fluid

Experimental Results

The system augmentation is primarily a result of the increased mass flow rate through the turbine. This increase in entrance velocity may be thought of as the combination of two major pressure effects. The first of these is the action of the diffuser. The

efficiency of this element is dependent upon such factors as the let configuration, number, and location of boundary layer energizing slots, size of the slots, and turbine disk loading.

The second effect is the diffuser exit plane static pressure reduction, the so-called C_{p_4} effect. The system parameters that affect this phenomenon are discussed in more detail later. The importance of this effect may be emphasized by realizing that a subatmospheric exit pressure requires that the exiting fluid continues to expand to the far downstream conditions. The corresponding further rise in static pressure is accomplished without the need (and cost) of constructing more diffuser structure. For 30 and 40°, typical values for the exit pressure coefficient, $C_{p_4} = (p_4 - p_1)/\frac{1}{2}\rho V_o^2$, are approximately -0.58 and -0.63, respectively. Although these reductions have the effect of doubling the power output relative to a C_{p_4} of 0, it is important to appreciate that the Betz one dimensional theory for an optimum conventional wind turbine implies that the equivalent C_{p_4} is -1/3 in that case as well. Therefore, a DAWT receives the net benefit in diffuser size reduction of only that C_{p_4} below the par value for the conventional machine, something like -0.2 to -0.3.

Figure 5 shows the standard measurements used to compute the augmentation ratio. Figure 10 shows a typical radial survey of several properties of the exit plane flow. First note that the static pressure does not vary greatly across the exit, when compared to its centerline value. Next note the structures of the dynamic pressure traces, showing clearly the acceleration of the external flow at the exit lip. The depressed pressure zones near the walls are indications that further development of this configuration is possible. If an exit plane profile produced a zero or negative value of dynamic pressure near the wall, it would be an indication

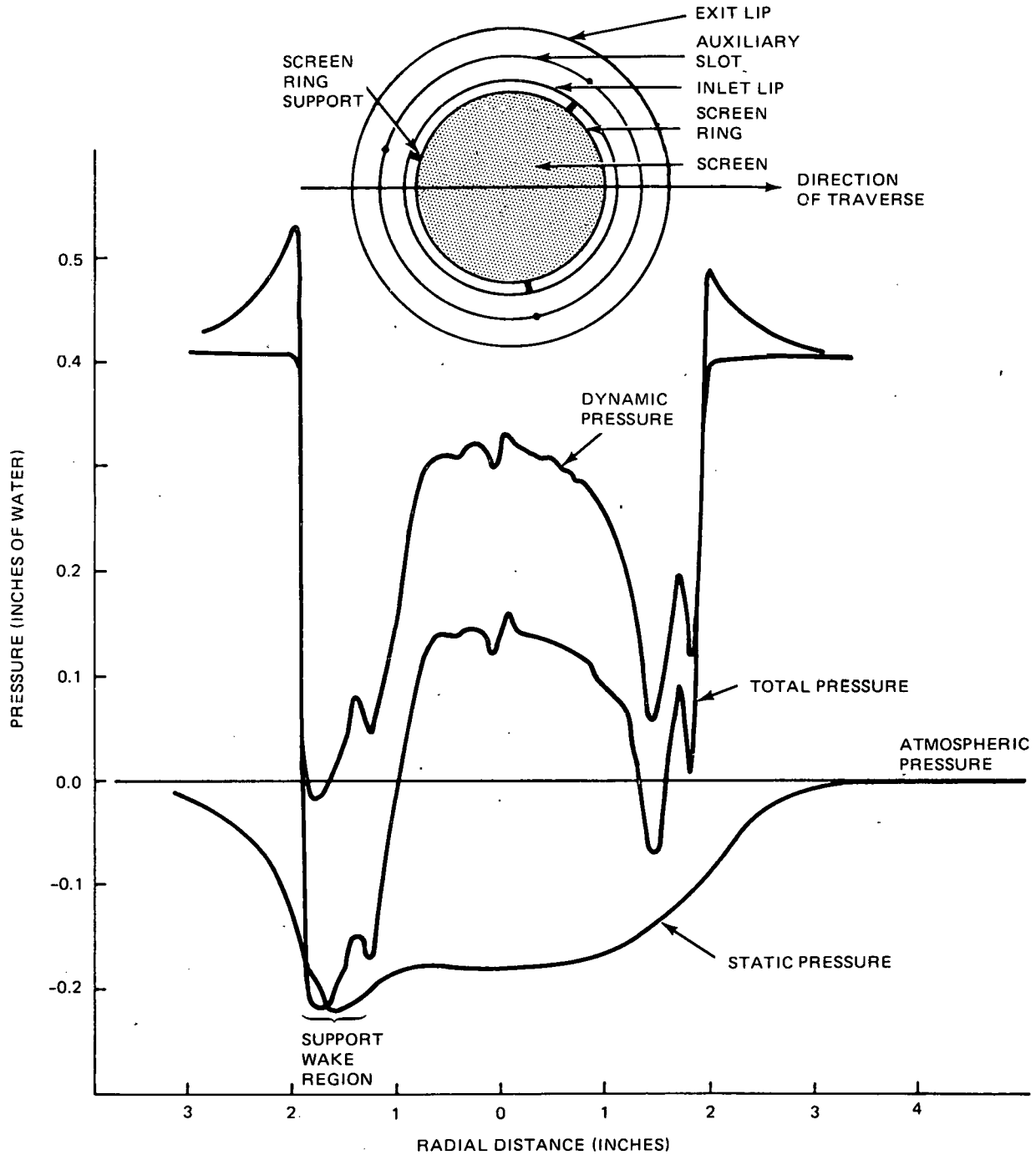

Figure 10 Radial Profiles at the Exit Plane of the Baseline Diffuser, C_T = 0.47

of a stall condition. This stall may actually exist outside the physical boundary of the diffuser because the flow is still recovering to atmospheric conditions. The secondary peaks near the walls represent the excess momentum supplied by the inlet slot as an ejector flow. Compared to Fig. 6, the diffuser action smooths the entrance profile. The slight asymmetric nature of the exit plane profiles is due to the wake region behind the screen ring support. The top (left hand side) of the trace passes nearly directly behind one of the three supports and manifests itself as a total pressure loss.

Many parameters have been identified that influence the diffuser system performance. Investigations were conducted to determine the effect of several of these. Although it was impossible to span the entire parameter space for each configuration, data were compiled that give an indication of the important trends.

Over 100 variations of wide angle segmented diffusers that employed the boundary layer control mechanism were constructed and tested. The conical half-angles chosen for those tested were 20, 30, 40, and 45°. The individual geometries ranged from area ratios (exit to turbine) of 1.63 to 4.94, and constructed of from one to four separate segments. Different turbine loadings were simulated by substituting screens with pressure drop coefficients between 0.37 and 0.93. Slot sizes between turbine and diffuser walls were varied from no slot to 0.1 in. and auxiliary slots from zero to 0.05 in. Only straight walled diffusers of the BLC type have been examined to date.

The first important result obtained for the diffuser component was associated with starting. If the flow in the diffuser was not properly started, it behaved like a jet issuing from a plane wall; that is, a vena contracta flow. Variation of the slot size had no

appreciable effect under these conditions since after flow separation from the wall, no amount of fluid injection would cause reattachment.

The solution was simply to move the screen up into a constant area section upstream of the diverging section, and to provide an initial inlet slot around the screen section which added enough momentum to the boundary layer to allow it to negotiate the starting angle of the diffuser as if it were a Coanda flow. That is, it appears necessary to provide an attachment surface of little or no divergence behind the screen before the diffuser begins to diverge rapidly or else jet flow will form.

Once it was discovered how to start the diffusers, parametric investigations were begun. Figure 11 shows the augmentation obtained from various angle diffuser configurations as a function of their area ratio. These diffusers were constructed from different numbers of sections with slots between them. It is apparent that the maximum augmentation seems to be at about an area ratio of three.

Increasing the area ratio beyond three always leads to a degradation of performance because the flow separates from the diffuser. For physical practicality, the boundary layer injection must be at discrete positions and cannot be continuous as in our mathematical model. In some cases, the separation point actually moves upstream when sections with increased wall area are added to the rear of the diffuser. Larger area ratios may be attainable, but they would require better implication of the slot boundary layer blowing.

For an area ratio of 2.78, 30 and 40° half-angle diffusers were tested with various simulated turbine disk loadings. This was accomplished by changing the screen solidity in the same diffuser configuration. An increase in turbine pressure drop usually causes

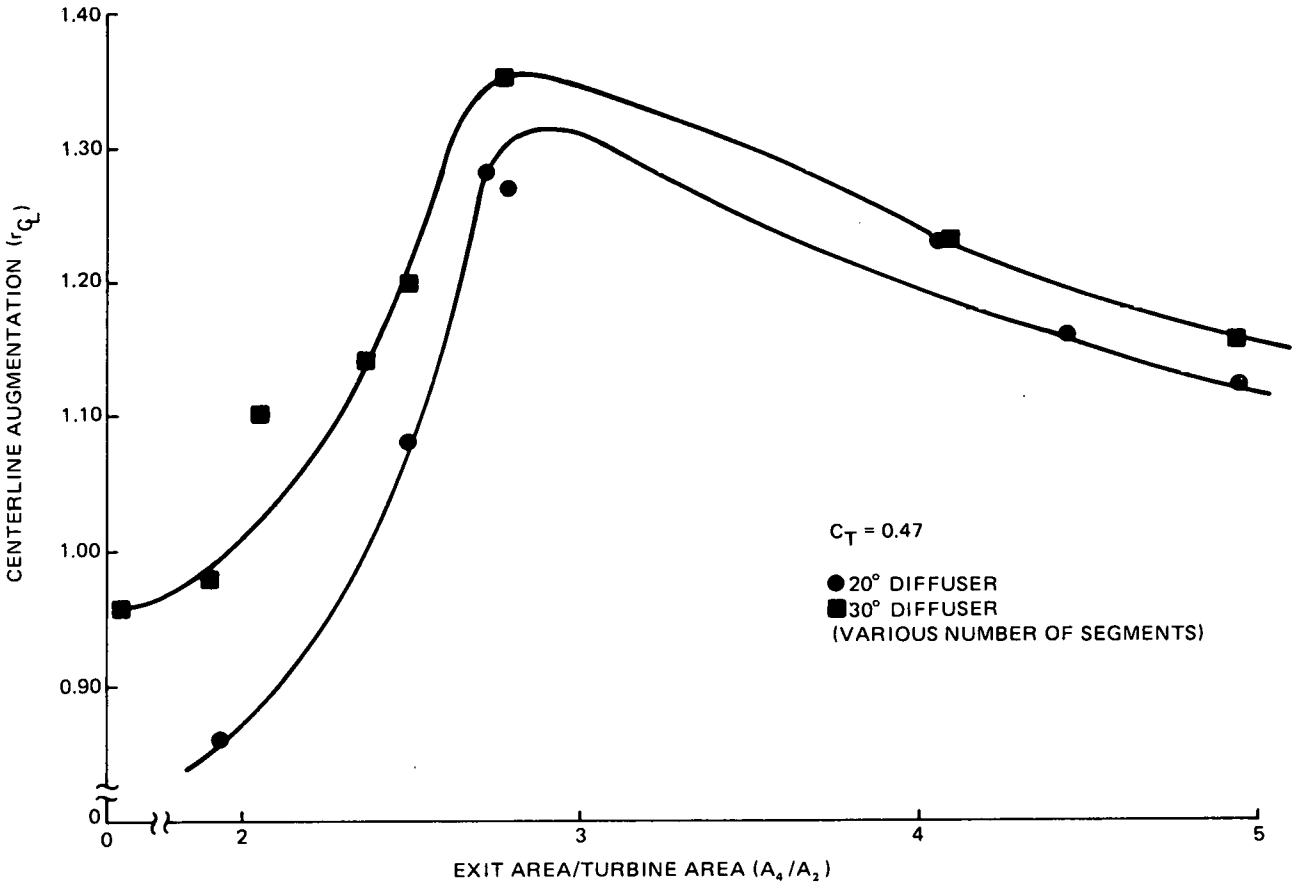

Figure 11 Trend of Centerline Augmentation With Area Ratio

the injection slots to perform better because the pressure differential driving the injection fluid across each slot is increased. However, the increase in blockage causes a greater resistance to the incoming fluid and a corresponding decrease in mass flow through the screen.

Figure 12 shows the dynamic pressure ratio induced ahead of the disk at various turbine loadings. In this range of loadings, the functional relationship is nearly linear. A linear least squares regression fit of the form $\bar{q}_2/q_o = A + BC_T$ was applied to the data. This allows for an empirical optimization with respect to loading which is equivalent to the optimization obtained from one dimensional

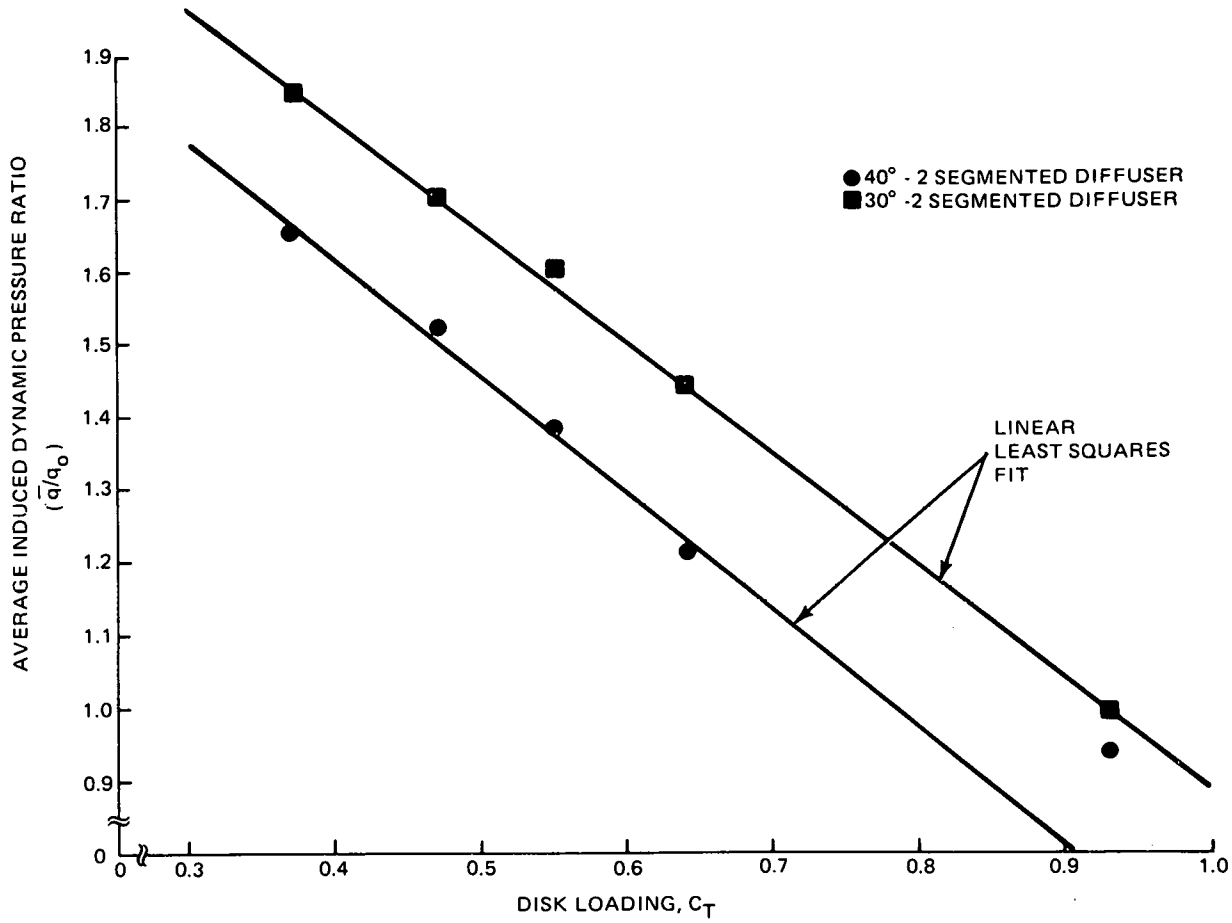

Figure 12 Average Induced Dynamic Pressure Ratio for 30° and 40° BLC Diffusers at Various Disk Loadings

momentum theory. The results are shown in Table 1, where the 40° diffuser calculations are based upon only the first four points shown in Fig. 12.

Figure 13 shows the results of augmentation ratio calculated from the measured average velocities in 30 and 40° diffusers. As expected, the best performance in both cases occurs very close to the empirically predicted optimal disk loading. The average augmentation ratio in these cases is the same as predicted to within experimental error. More importantly, however, the empirical prediction for the optimal disk loading coefficient, C_{T_o}, is in very good agreement with the loading predicted by the ideal one dimensional

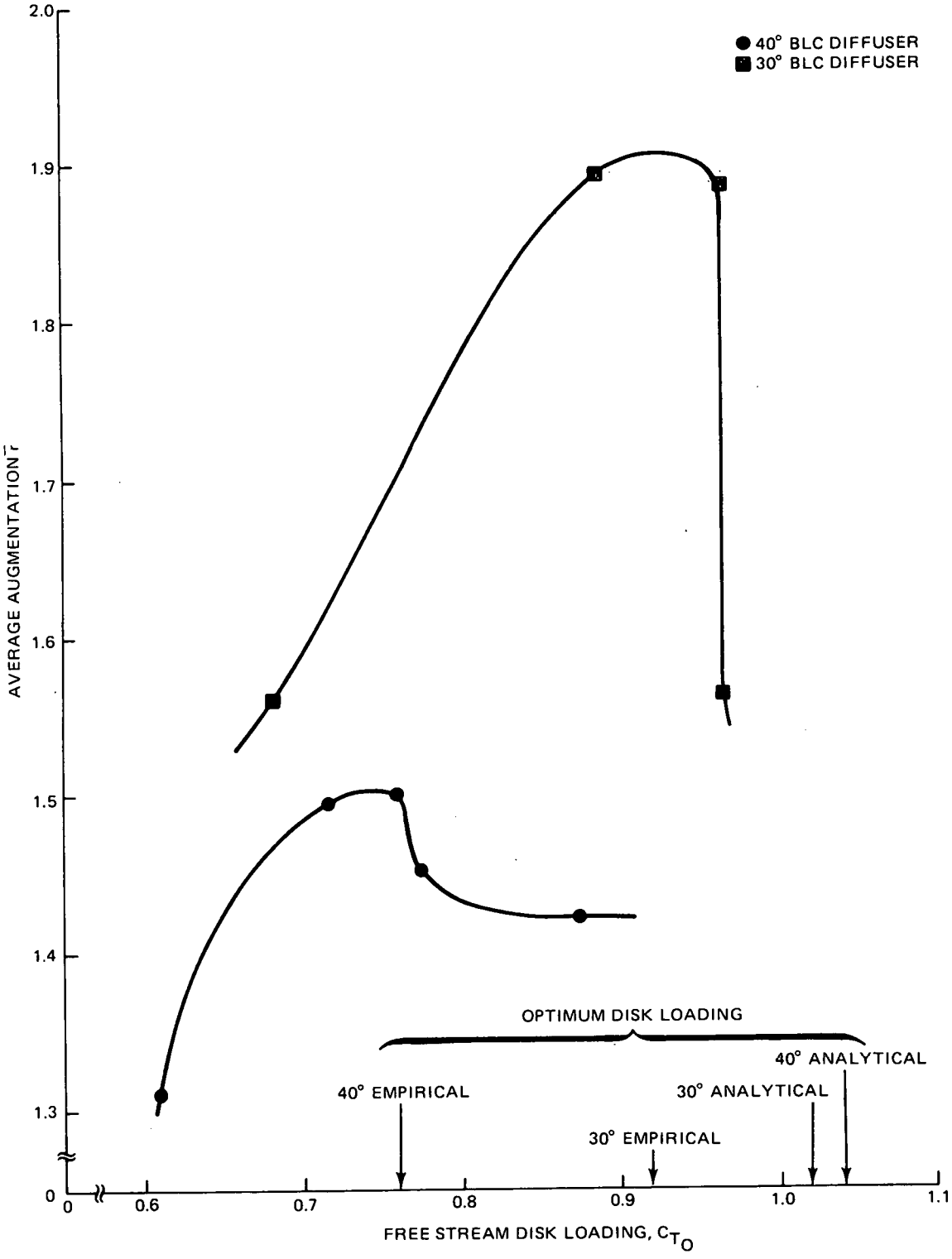

Figure 13 Dependence of Augmentation on Disk Loading From Experiments and Analysis

TABLE 1 EMPIRICAL OPTIMIZATION WITH RESPECT TO DISK LOADING OF 30 and 40° BLC DIFFUSERS

Diffuser Half-Angle	30°	40°
A	2.422	2.259
B	-1.529	-1.616
$(C_T)_{opt} = -\frac{2}{5}\frac{A}{B}$	0.634	0.559
$(\bar{q}_2/q_o)_{opt}$	1.453	1.356
$\bar{r}_{opt}$	1.87	1.49
$(C_{T_o})_{opt} = C_T(\bar{q}_2/q_o)_{opt}$	0.921	0.758
C_{P_4} at $(C_T)_{opt}$ (see Fig. 17)	-0.54	-0.56
C_{T_o} from Eq. (8) for $K_i = 0$	1.02	1.04

momentum theory [Eq. (8)]. The slightly higher values obtained from the momentum theory are due to the nonideal nature of the flow. This departure is larger for the 40° than for the 30° diffusers. The non-one dimensional nature of the flow resulting from the friction induced separate stall region is more severe in the 40° diffuser flow. After the relatively flat range of maximum augmentation, there is a very rapid loss of augmentation with a very slight increase in free stream disk loading. This is primarily a result of the decrease in induced flow through the turbine at local disk loading coefficients greater than the optimum.

A 30° half-angle diffuser with a screen factor (disk loading) 0.55 is the best configuration tested, giving a weighted average augmentation ratio of 1.89. We expect that it will be possible to improve upon this value. However, since this is a real diffuser geometry with demonstrable augmentation ratio values, it will be used for the cost estimates that appear later.

There are several conclusions that may be made regarding the number, size, and arrangement of diffuser segments and the characteristics of inlet and auxiliary slots. Decreasing the initial inlet slot by increasing the screen diameter in the same diffuser configuration is equivalent to increasing the apparent blockage which produces a slight decrease in the mass flow. However, the induced velocity, and therefore available local power density, increases towards the periphery. As a result, the decrease in system augmentation due to the reduced slot size was nearly compensated by the increase in turbine area, such that the total available energy to the turbine remained nearly constant. These data are shown in Table 2.

TABLE 2 TOTAL AVAILABLE ENERGY TO THE SYSTEM AS A FUNCTION OF SLOT CONFIGURATION

Inlet Slot Area/Turbine Area	Auxiliary Slots	Augmentation ($\bar{r}$)	Total Turbine Power (Arbitrary Units)
0.245	1	1.76	5.45
0.113	1	1.58	5.47
0.055	1	1.46	5.22
0	0	1.10	4.40
0.245	0	1.36	4.21

It is possible, therefore, to reduce the inlet slot substantially before the decrease in system augmentation is no longer compensated by the increase in turbine size. Decreasing the turbine size with respect to the diffuser increases the system augmentation. The inlet fluid is not only used to energize the boundary layer so that it may negotiate the starting turn into the diffuser, but the inlet now also behaves like an ejector, with high energy fluid in the peripheral slot drawing more fluid through the turbine. If increasing the diffuser size were less expensive than increasing the turbine diameter, promoting the ejector system may become more economically credible.

A series of tests were conducted using 30° half-angle diffusers to determine the effectiveness of the slots. When a no-slot configuration was compared to the same diffuser with a 24.5 percent inlet slot, an increase of 24 percent in augmentation was found (note that the increase in inlet slot was at the expense of turbine area).

Figure 14 shows the augmentation possible from single segment diffusers as a function of area ratio. The trend seems to indicate the best performance near an area ratio of three. This is partially a result of the C_{p_4} effect, still to be discussed, and also the failure of the fluid to remain attached to the diffuser walls for that distance without aid.

For an area ratio of 2.78, the addition of a single auxiliary slot increased the augmentation by another 23 percent. The exact positioning of the auxiliary slot seems to have a minor influence as shown in Fig. 15. Moving the slot forward from 52 percent diffuser length to 39 percent increased the augmentation 16 percent. Further forward movement to 30 percent length again decreased the

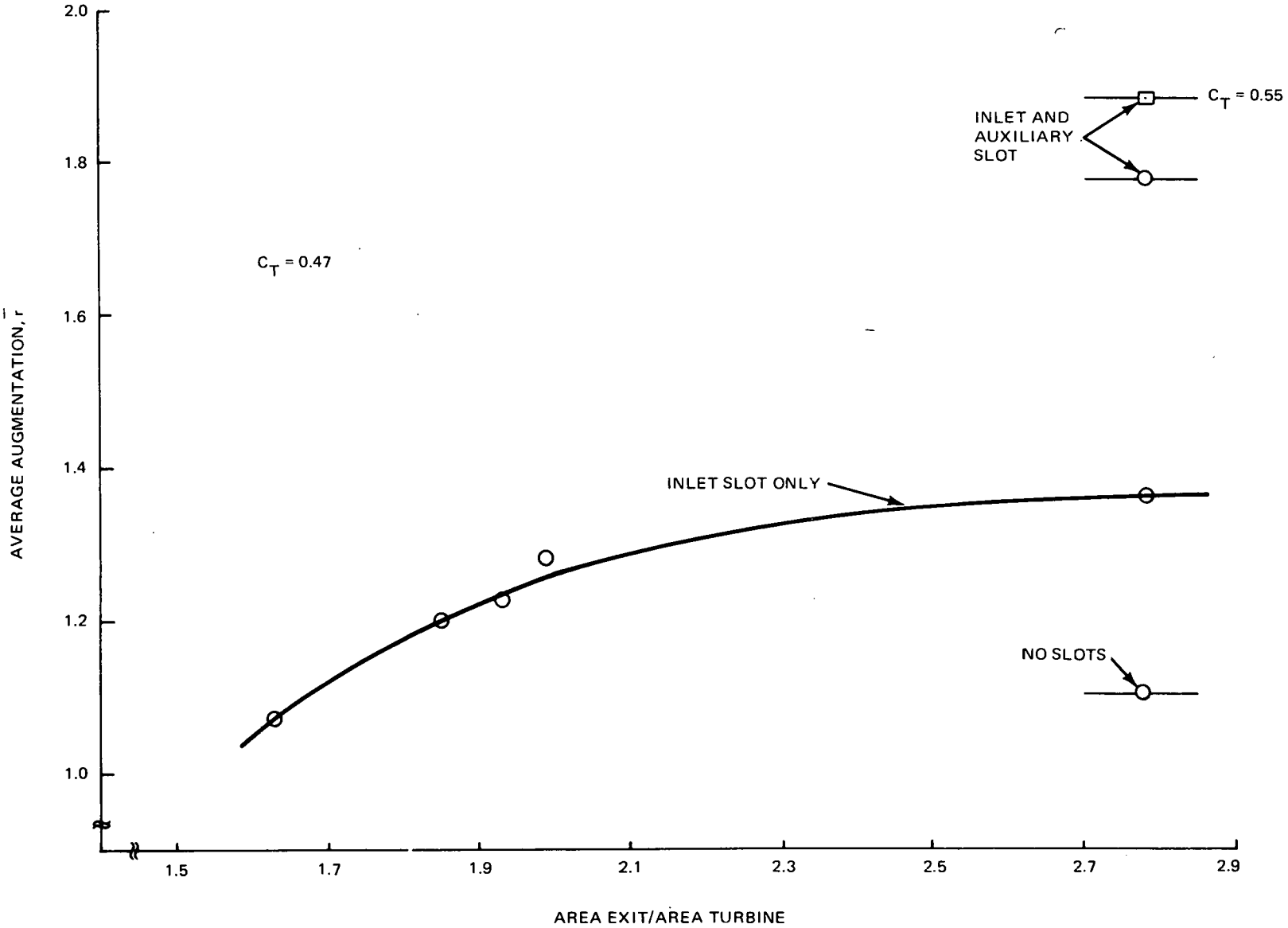

Figure 14 Effect of Slot Configuration on Average Augmentation in 30° BLC Diffusers

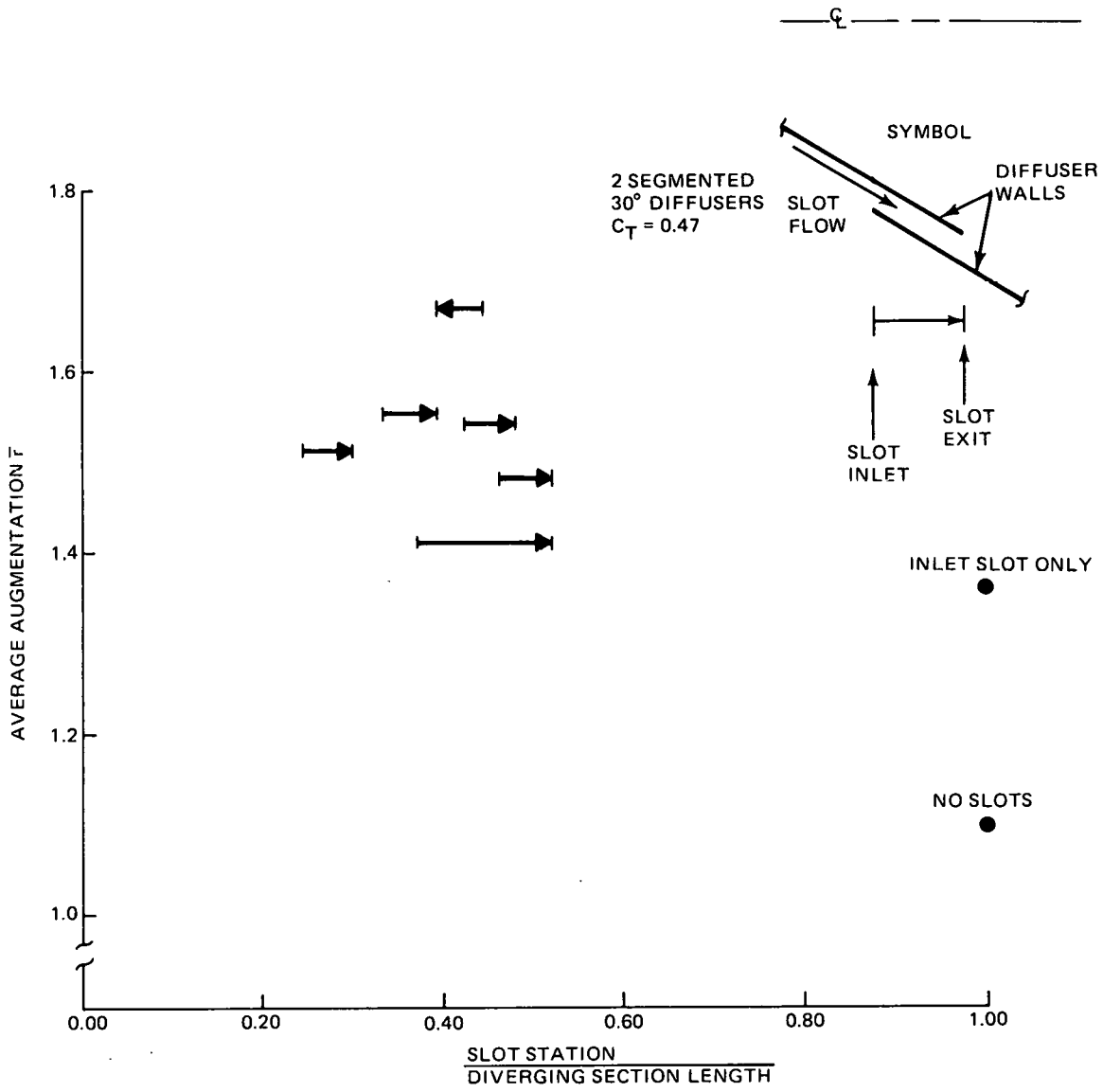

Figure 15 Effect of the Second Slot Position on Augmentation

augmentation because the second section is too long for the re-energized fluid to overcome. In this case, to maintain the same length a second auxiliary slot is indicated. Alternatively, the diffuser could be made shorter.

Shown on the same Fig. 15, are two cases designed to test the effect of the slot length, that is, the slot loss coefficient K_s in Eq. (17). For virtually no length of slot, there was an 8 percent increase in augmentation compared to a 5 percent loss in

the exceptionally long slot. In the few cases tested, there did seem to be too much effect of changing the slot height.

No general statement may be made regarding the "correct" number of segments as a function of chosen area ratio. Diffusers with the same angle and area ratio but constructed from a different number of segments were compared. For some particular area ratio, the best performance was obtained with two segments, but an increase to three resulted in degraded augmentation. At higher area ratios, three sections seemed best with poorer performance with both two and four sections. As indicated earlier, the optimum configuration will probably be determined by a tradeoff between the number of sections and the exact positioning of auxiliary slots.

A smooth inlet contour was created by the use of modeling clay. It appears that the clay fairing along the inside surface of the inlet resulted in a slight initial diffusion of the flow prior to its entrance into the simulated turbine. The result was that a fraction of the available boundary layer momentum was dissipated during this process and the over-all diffuser performance degraded. Simply removing the clay from the inside of the inlet increased the augmentation ratio by 23 percent. In the other direction, for another configuration, the effect of selectively sharpening the leading and trailing edges of a two-segmented 30° diffuser was examined. As seen in Table 3, the best configuration is probably one with relatively blunt edges. The sharper edges may have a tendency to create local large adverse pressure gradients and therefore separation. In an auxiliary slot, this stall would effectively block the slot.

The exit plane static pressure effect is very important to the action of the system. As seen by the theoretical Eqs. (6) through (8), the value of the exit plane static pressure coefficient is an

TABLE 3 EDGE CONDITION EFFECT ON AUGMENTATION

Blunted Edges (See Diagram)	$\bar{r}$	$(\bar{r}_{max}/\bar{r}) - 1$
None	1.28	0.203
1	1.30	0.185
1, 2	1.39	0.108
1, 2, 4	1.43	0.077
1, 2, 3, 4	1.54	0

Edge Notation

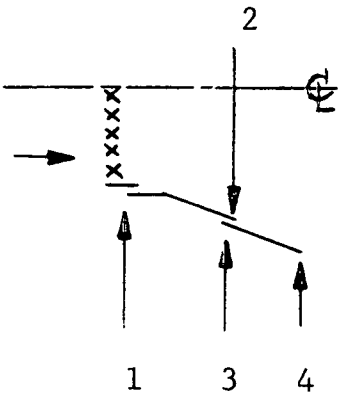

important parameter in the system optimization. Almost independent of the specific performance details of the diffuser, the exit plane subatmospheric pressure translates the entire diffuser pressure profile linearly, such that the base pressure is nearly diffuser performance independent. The total system augmentation is not only due to the diffuser characteristics but also (and in some cases, more so) to this base pressure reduction. A brief discussion appears later that summarizes our hypothesis about the physical mechanism of the C_{p_4} effect. The following presents some empirical data found for C_{p_4}.

Initially, it was expected that C_{p_4} would be a function of the diffuser area ratio. For very small area ratios, as seen in Fig. 16, this seems to be the case. However, for a particular diffuser angle and disk loading, a size is quickly reached where C_{p_4} remains essentially constant with increasing area ratio. When very large area ratios are reached, the C_{p_4} effect actually decreases due to the substantial separated stall region. The area ratio where C_{p_4} becomes asymptotic and the particular magnitude is very dependent on diffuser angle. Smaller angles asymptote at larger area ratios and at lower subatmospheric pressures.

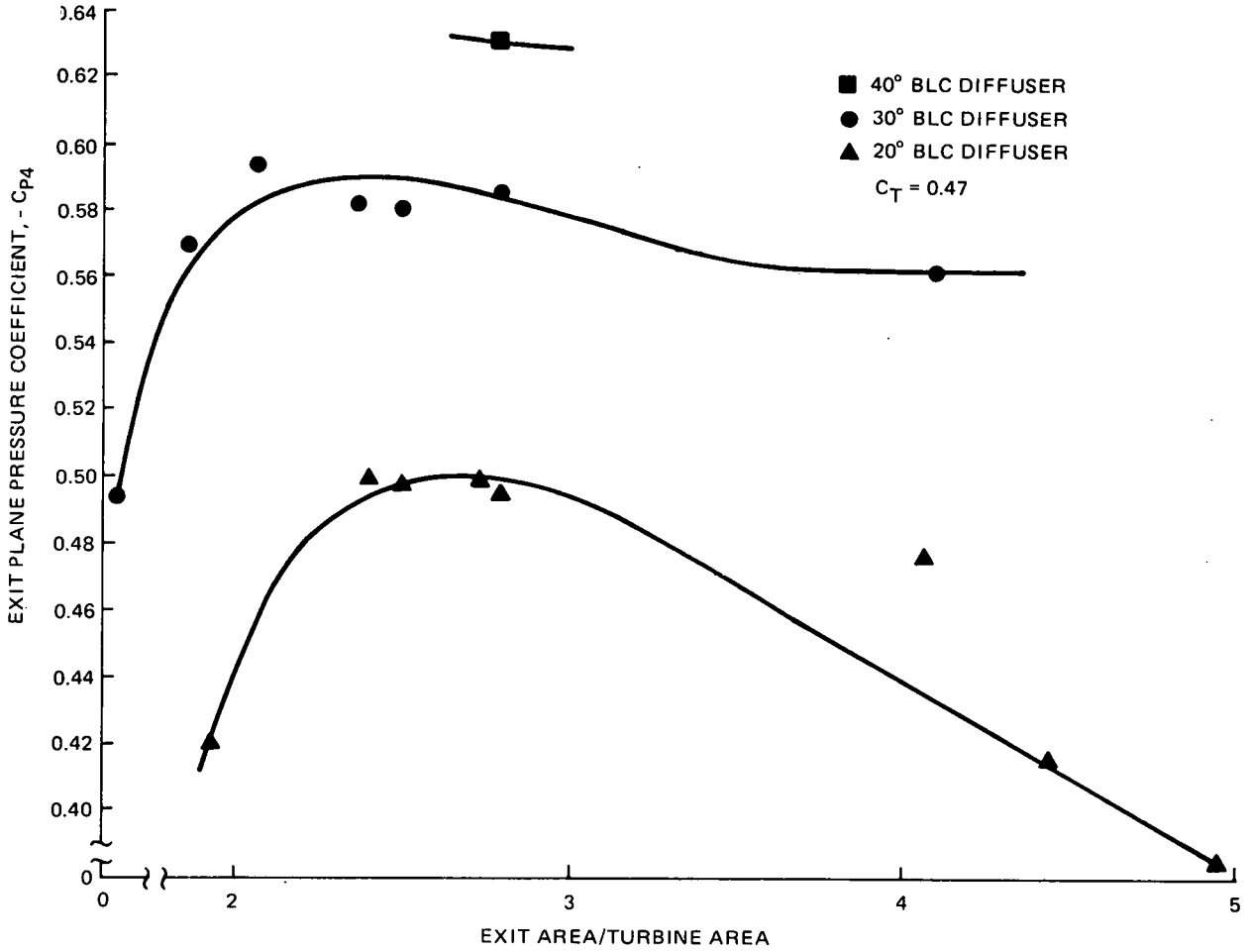

Figure 16 Exit Plane Pressure Reduction for Various BLC Diffuser Half Angles as a Function of Area Ratio

When the value of C_{p_4} was compared to the turbine (screen) disk loading coefficient for a particular area ratio, Fig. 17, a strong dependence was found. The disk loading which gives the lowest base pressure seems to be a function of the exact configuration employed. The value of the loading does not seem to be too different from that found to give the best performance (see Fig. 12), thereby further emphasizing the advantage that the C_{p_4} effect gives.

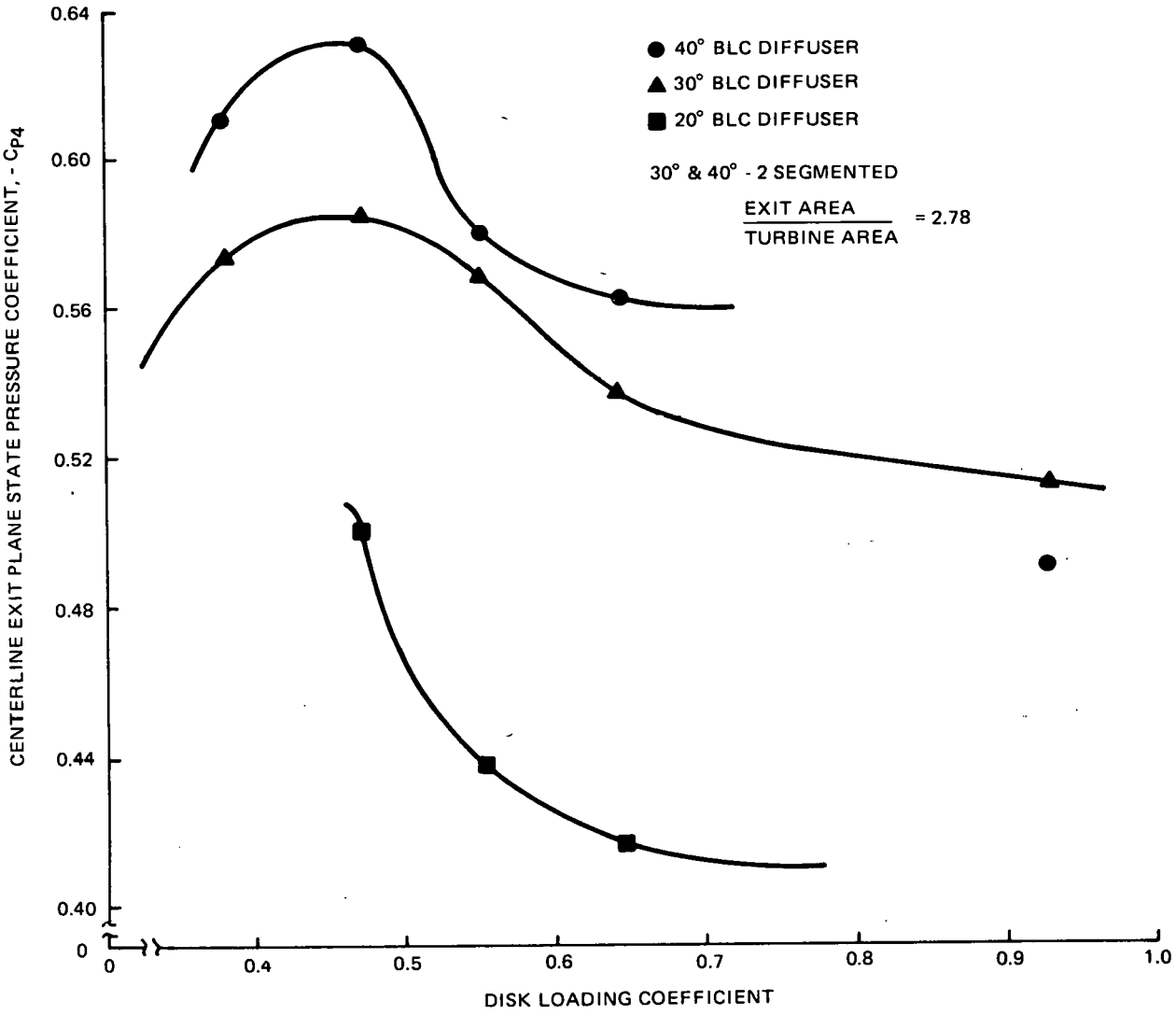

Figure 17 Exit Plane Pressure Reduction for Various BLC Diffuser Half Angles as a Function of Disk Loadings

Since the C_{p_4} advantage works nearly independently of the diffuser, increased augmentations can be achieved if the area ratio used is small enough that the asymptotic value of C_{p_4} has not been reached. With respect to the external flow field, the appearance of a larger area ratio can be simulated by using a flap. For example, in a 20° diffuser with a flat plate flap deflected 90° radially outward, centerline augmentation was increased 8 percent. The length of the flap was 15 percent of the diffuser length.

Because the proposed design concept calls for the diffuser exit lower lip to be supported from the ground, it is very important that the proximity of the ground does not degrade the system performance. An examination of this problem was made. A ground plane was constructed of 1/8 in. aluminum and supported upside down in the flow by the jet exit plane collar. The models were suspended at various heights by threaded rod supports which passed through the ground plane. With no model, the viscous boundary layer was evident (90 percent point) in the dynamic pressure profile to about 0.6 in. above the plane. The static pressure effect was obvious to only about 0.4 in. above the plane.

In model tests, the upper portion of the diffuser showed a very slight increase in mass flow when compared to the same diffuser configuration with no-ground plane. However, the lower section, nearer to the ground, exhibited a substantial improvement. With the tail of the diffuser on the ground, the lower section augmentation increased by 10 to 14 percent. Even when the tail was half a turbine diameter above the ground, the lower section still showed about a 6 percent better augmentation than for the no-ground plane case.

This increase may be due to the distortion of the exit plane static pressure profile, the C_{p_4} effect. However, no evidence of

this is apparent from exit plane static pressure surveys. The important point, which cannot be overemphasized, is that there is no apparent degradation; actually, there is a slight increase in system performance in the presence of a ground plane.

The other important consequence of real ground is that the velocity profile far upstream of the system is no longer uniform. An atmospheric boundary layer was simulated in the jet facility by a honeycomb mesh. A length of cellular section produces a total pressure drop due to friction. The longer the section the larger the pressure drop and, therefore, the smaller the resulting dynamic pressure. The honeycomb was cut with a linear profile which produced a nearly linear dynamic pressure profile. The honeycomb was installed 7 in. upstream of the jet nozzle exit. The total profile did show some characteristic jetting at the boundaries absent from the usual exit flow profile.

The model was located 2 in. downstream of the jet exit. At this position, the turbine disk intercepted a velocity profile at infinity which varied by 14 percent. The augmentation calculations were based upon the integrated available power in this intercepted disk.

In the presence of the shear flow, there was a very slight decrease of augmentation. At all the measured local positions, there was a loss of about 1 percent of the augmentation of the same configuration mounted in a free jet flow. This is very near the resolution capabilities of the instrumentation.

As a final test, the combination profile of the ground plane and shear flow was tried. The resulting flow field appeared to be a simple superposition of the individual profiles. Again, the upper part of the diffuser showed little effect, while the lower section indicated about a 7.5 percent increase in augmentation

when based upon an integrated value of q_o. The local augmentation is about 11 percent greater than the free jet diffuser augmentation. The important result, however, is that there appears to be no decrease in the augmentation effect of the diffuser system.

Another important aspect of a real turbine geometry is the presence of a centerbody. A comparison was made with and without centerbodies at a single representative point (at 60 percent of the radius). Seven different diameter centerbodies were available for the tests ranging from an area of centerbody to area of turbine of 1.9 to 30.9 percent. Two forebody designs were used: a sharp and a blunt leading edge, each 1/2 in. long and of the same diameter as the afterbody. The afterbodies were circular cylinders of various lengths from 1/2 to 4 in. and all tests were conducted in a 30°, two-segmented diffuser with a 16 mesh/in. screen.

A portion of the test matrix is shown in Table 4 where the measurement system precision is about 1 percent. When the area of the centerbody was less than about 8 percent of the total disk area, a very slight degradation of performance was apparent (less for longer centerbodies and more for the sharp forebody). Flow visualization techniques indicate that the fluid remained firmly attached to the centerbody and quickly flowed in behind it. This produced only a very small wake region which was undetectable by exit plane pressure surveys. However, at the next available centerbody size (area ratio of about 12 percent) and for short afterbodies, the flow reverted to a highly transitory flow. By increasing the afterbody length, or using a sharp forebody, converts the severely oscillating flow into a stable annular jet moving along the diffuser wall with a large, conical diverging center wake.

Two other separated flow configurations were achieved for the 8 percent centerbody. When a blunt forebody was combined with a

TABLE 4 PORTION OF THE CENTERBODY TEST MATRIX

Area Centerbody/ Area Turbine	Forebody	Afterbody (in.)	Δr at 60% Radius
0.03	blunt	1/2	0.012
	"	1	0
	"	2	0.024
	sharp	1/2	0.037
0.077	blunt	1/2	0.012
	"	1	0
	"	2	0
	sharp	2	0.012
0.121	blunt	1/2	0.073
	"	1	0.073
	sharp	1	0.202
0.077	blunt	sharp	0.072
	sharp	blunt	0.648

sharp afterbody, the flow separated from the afterbody, and lead to a 7 percent decrease in augmentation. When a sharp forebody was combined with a blunt afterbody, the flow separated from the forebody and did not reattach itself to the centerbody, but continued to diverge for a 65 percent decrease in local augmentation.

The presence of a centerbody requires the centerline mass flow be diverted into a larger annular ring. For the smaller bodies, the mass flow at the representative point remains essentially unchanges implying no loss of augmentation. However, there will exist a larger mass flow at a radial station corresponding to the radius

of the centerbody than without a body. For larger bodies, there a loss of diffuser performance manifested as a decrease in flow rate. This interpretation must be examined more fully by complete radial surveys.

Two final points are important. In the system configurations that have been found to give the best performance, flow visualization techniques indicate three distinct conical regions of low velocity fluid (see Fig. 10). These may be traced directly to the pins which support the center screen ring. It is unclear, however, whether the losses are inherent to the system and simply manifest themselves at the weakest point or whether they are purely a cylindrical wake effect. If the latter, streamlining the support rods in larger scale models should improve the situation.

The other point is that in all cases tested, there did not seem to be any indication of severe diffuser flow variations with small changes in either pitch or yaw. It is expected that as the inlets to the turbine as well as the diffuser are improved, there would be even less of a tendency of yaw-induced distortion.

RING WING DIFFUSER

The suggestion of ring wing diffusers for WECS was made in the early 1960's (Ref. 5). The concept is based on the fact that airfoil contours exhibit a generally low pressure field along the upper surface and a high pressure field along the lower contour. In a ring diffuser configuration, the inner surface corresponds to the low pressure side. The airfoil section lift acts towards the centerline and creates a reaction force on the internal flow that tends to direct it radially outward as well as axially downstream. The circulation induced around the lifting airfoil section results in an increased flow rate through the upstream end of the diffuser compared

to a simply cylindrical duct of the same cross sectional area. Therefore, a turbine that is positioned within the ring wing diffuser has an augmented mass flow passing through it and can extract more power than a bare turbine. A consequence is that very high lift airfoil section configurations appear to hold the most promise.

The aerodynamic characteristics of two dimensional airfoil sections undergo modification in the ring-wing configuration depending on the aspect ratio (AR) (= diameter/chord) of the ring. For AR greater than 1.5, or the high AR range, the aerodynamic center of the airfoil moves rearward, and the lift coefficient, C_L, is greatest at angles of attack, α, between 15 and 20°, but breaks and sharply drops downward at higher α's (Ref. 6). The wake vortices in high AR rings move very little in a lateral direction. In keeping with our objective of short cost effective shroud designs, we have examined principally high AR geometries.

Three basic airfoil contours have been employed for ring-wing diffusers: a) the moderately thick NACA 4412 section (Ref. 7); b) the high lift Williams airfoil "A" (Refs. 8 and 9); and c) the high lift, Liebeck laminar rooftop design (Ref. 10). The NACA 4412 designation signifies a maximum thickness of 12 percent of the chord length and a 4 percent of chord maximum camber at a position 40 percent of chord downstream from the leading edge. This 4412 contour was used for single wing rings at attack angles, α, of 6 and 12°, producing theoretical C_L values of 1.2 and 1.9, respectively; for a double element assembly combining a 6° main airfoil and 12° flap, theoretically producing a maximum pressure coefficient $C_{p_{max}} = (p - p_o)/q_o$ of -8.5 at the inner surface near the leading edge (the single element 6° airfoil has a $C_{p_{max}} = -2.6$, and the single 12° airfoil has a $C_{p_{max}} = -7.8$);

and also for single airfoil elements with a split (trailing edge) flap of 20 percent chord length. (These flaps should theoretically increase basic section $C_{L_{max}}$ by 50 percent and move the center of pressure downstream of that for the unflapped airfoil.)

The Williams A contour gives a theoretical C_L at $\alpha = 0°$ of about 2.8. Used with a 30° deflection airfoil type flap (60° of mainchord length) it should produce a C_L of 3.5 and a minimum C_p of -7.8 near the inner leading edge of the two element assembly. With a 20 percent chord split flap the main element C_L should reach about 4.0 at $\alpha = 0°$.

The Liebeck contour is a specially designed shape for producing a broad plateau of low and nearly constant pressure over the upper surface. The shape we have considered yields a steady C_p of -5.2 over 25 percent of the chord length and a C_L of 2.54 without auxiliary lift devices.

Although theoretical pressure fields can be calculated around these airfoil contours, when a screen or a turbine is introduced in proximity to the airfoil, the resulting nonisentropic conditions alter the conventional computational problem and the equations must be reformulated in order to yield valid flow field predictions. This analytical work will be undertaken as part of the second year activity of this project.

The effect of energy extraction by a turbine or energy dissipationbby screen drag on the ring-wing diffuser flow field has been investigated empirically during the present contract period. Various screen solidities were used to simulate different turbine actuator disk loadings, and were mounted at several axial positions relative to the diffuser throat (minimum cross section) to study the interaction with the internal flow field.

Table 5 summarizes the geometric features of the ring-wing diffuser models actually tested. On the basis of aspect ratio model 2 is the shortest diffuser, but the Williams A contour design (model 3a) requires the least amount of material, based on the normalized surface area values. The experimental augmentation ratio data presented in the next section provide a means for estimating the relative cost effectiveness of these short geometry diffusers.

Theoretical Considerations

The calculation of pressure and velocity distribution along the surface of a cambered airfoil by conformal transformation of a Z-plane circle into a wing section is well known (see, for example, Ref. 11). This method has been programmed for digital computers so that for any set of airfoil section coordinates along a chord line and a specified stream velocity, the local surface velocity and pressure coefficient can be obtained. The inviscid theoretical results approximate measure surface pressure distribution along the wing section until the stall limit is approached.

In one case, at a nonzero angle of attack, α, the upper surface of the NACA 4412 airfoil has a highly negative pressure distribution from almost immediately downstream of its leading edge to about the 95 percent chord point. Pressures above ambient static prevail along the rear 5 percent of the upper surface and all along the bottom surface. The upper surface in our ring-wing design faces the inner axis of the diffuser. We have computed the flow fields for α ranging from zero to 18°.

At a distance from the upper surface, the flow field also has subatmospheric pressure. For the NACA 4412 at $\alpha = 6°$, this pressure reduction still is more than half of the surface value at a

TABLE 5 SUMMARY OF RING-WING DIFFUSER GEOMETRIES

Model Configuration	Airfoil	Chord c (cm)	Throat Diameter (cm)	Aspect Ratio AR	Surface Area, SA (cm^2)	Total Enclosed Volume (cm^3)	SA/D^2	$A_{exit}/A_{turbine}$	Section Angle of Attack α(°)	Flap Option	Flap Deflection Angle
1	NACA 4412										
	a)	3.71	6.10	1.64	267.74	24.50	7.2	1.47	6°	None	—
	b)	"	"	"	303.23	26.06	8.2	2.14	"	Split 20%c	$0 < \delta < 90°$
	c)	6.99	"	0.87	638.71	61.62	17.2	2.65	"	NACA 4412c 98% c	$\delta = 6°$
2	NACA 4412										
	a)	3.65	8.00	2.19	374.19	37.44	5.8	1.54	12°	None	—
	b)	"	"	"	418.71	39.00	6.5	2.05	"	Split 0.2c	$0 < \delta < 90°$
3	Williams										
	a)	2.69	5.08	1.89	100.64	21.79	3.9	1.56	0°	None	—
	b)	"	"	"	130.97	23.11	5.1	2.10	"	Split 0.2c	$0 < \delta < 90°$
	c)	4.06	"	1.25	201.94	34.25	7.8	3.24	"	Airfoil 0.6c	$\delta = 30°$
4	Liebeck (laminar rooftop)	4.57	5.33	1.17	273.55	59.65	9.6	3.63	0°	None	

radial distance of 20 percent chord. This characteristic becomes very important in locating the first ring diffuser section relative to the turbine exhaust. Theoretically, more mass flow will be forced through the turbine if lower pressures can be maintained downstream of it.

A second factor in assuring stable subatmospheric pressure at the turbine exhaust is to eliminate any large pressure rises above atmospheric levels along the interior surface of the ring diffuser. Such a condition could exist near the trailing edge of the 4412 airfoil for low α. To reduce this pressure we can stage a second ring wing, with slight axial overlap, around the first or use a flap to increase effective camber of the basic airfoil. The two element airfoil has a resulting pressure field that depresses considerably the low pressures along the upper (inner) region of the wing ring. This helps to maintain a good diffusion process for high augmentation.

Other factors influencing the wing diffuser design are the effective diffuser expansion ratio and over-all length-to-initial diameter ratio. Both of these items can be varied by selection of the angle of attack of each of the staged rings and their aspect ratios (average diameter/chord). For given aspect ratios, higher expansion ratios and shorter length diffusers can be obtained by going to higher α, up to the airfoil stall condition.

Experimental Results

The ring wing models were machined from aluminum on a tracer lathe using templates of the airfoil section, and final-finished by hand. Multielement diffusers (e.g., models 1c and 2c) were assembled with brass pins to produce equidistance gaps between the flaps and airfoil. The models were supported externally in the airstream by three brass radial rods implanted into the diffuser

body and clamped to three threaded bars running axially from the ility nozzle flange, outside the flow channel.

Screens which simulate the turbine pressure drop were mounted in the internal flow. A short, constant area, stainless steel ring was suspended coaxially within the diffuser by brass pins protruding radially from the duct wall. Alternatively, the screen was epoxied directly to the diffuser wall by three thin interwoven wires acting as extensions of the screen circle.

Two typical centerline surveys of static and total pressure for ring wing diffusers are shown by Figs. 18 and 19. Figure 18 shows pressure traces for the NACA 4412, $\alpha = 6°$ contour ring wing with a 20 percent chord split flap deflected 90° outward (see item 1b of Table 5 for details). Figure 19 is for the Williams A airfoil contour with a 20 percent chord (see item 3b of Table 5 for details). In the case of Fig. 18, the screen that simulates a wind turbine is mounted at the theoretical minimum pressure location along the airfoil surface. The screen and its attachment result in an effective disk loading of $0.83\ q_2$. This is indicated by the total pressure, P_T, survey (lower part of Fig. 18) showing a virtually constant value of 42 units (with respect to atmospheric pressure) prior to the screen, a sudden drop to about 2 units, and a final pressure recovery to about 12 units at a distance equal to about 20 mesh heights (1.5 cm = 0.6 in.) downstream of the screen. The continued decrease of total pressure much further downstream indicates the mixing loss processes in the ring wing's wake. The static pressure survey (upper part of Fig. 18) shows an inlet static pressure of 6 units above atmospheric, or a local dynamic pressure, q_2, of $0.85\ q_o$ just upstream of the screen simulator. The static pressure drop accompanying the total pressure loss through the screen is slowly recovered in the remainder the ring wing diffuser section to yield an exit pressure

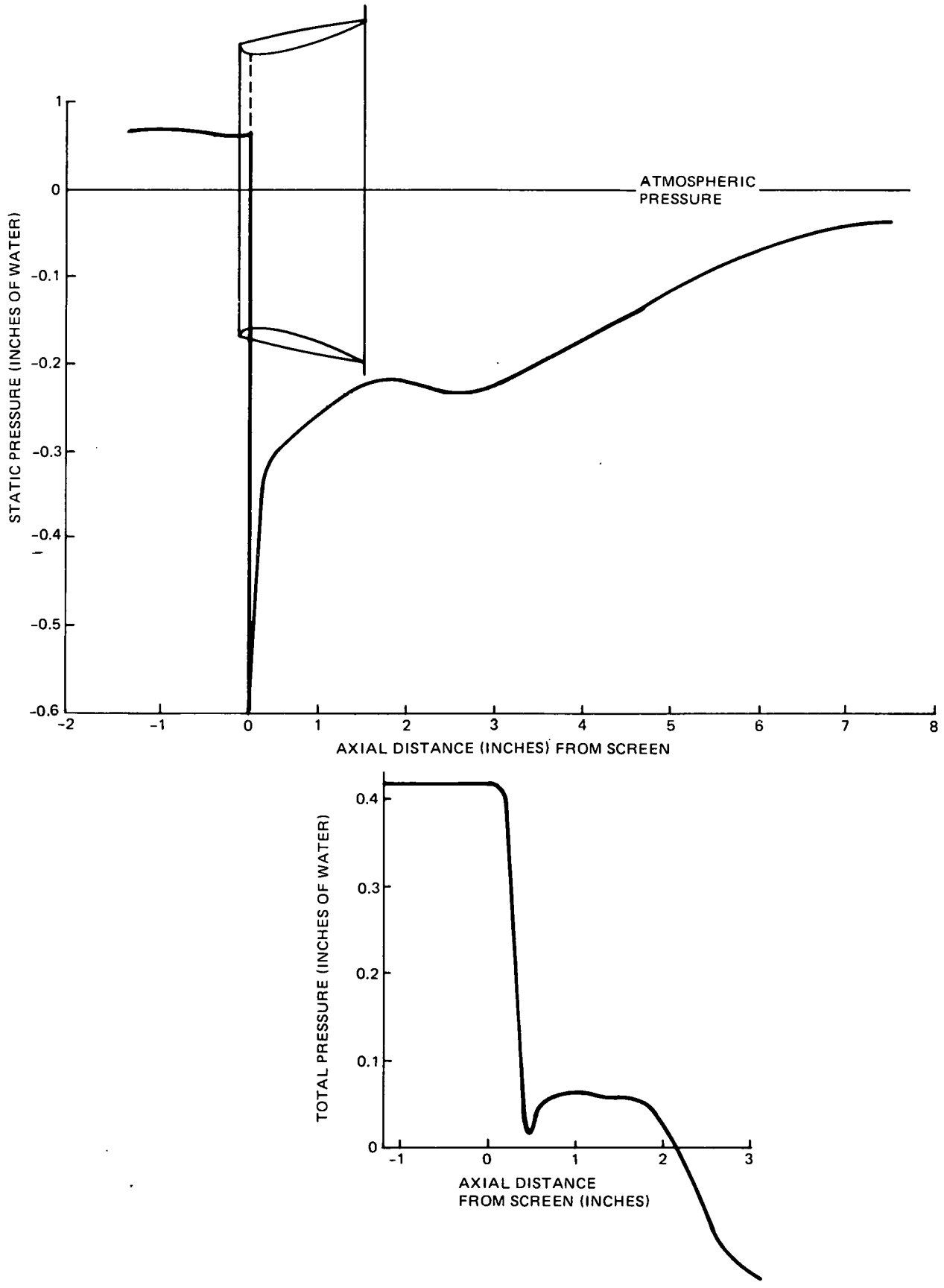

Figure 18 Typical Centerline Axial Static and Total Pressure Surveys of a Flapped NACA 4412 Contour Ring Wing Diffuser, $C_T = 0.83$

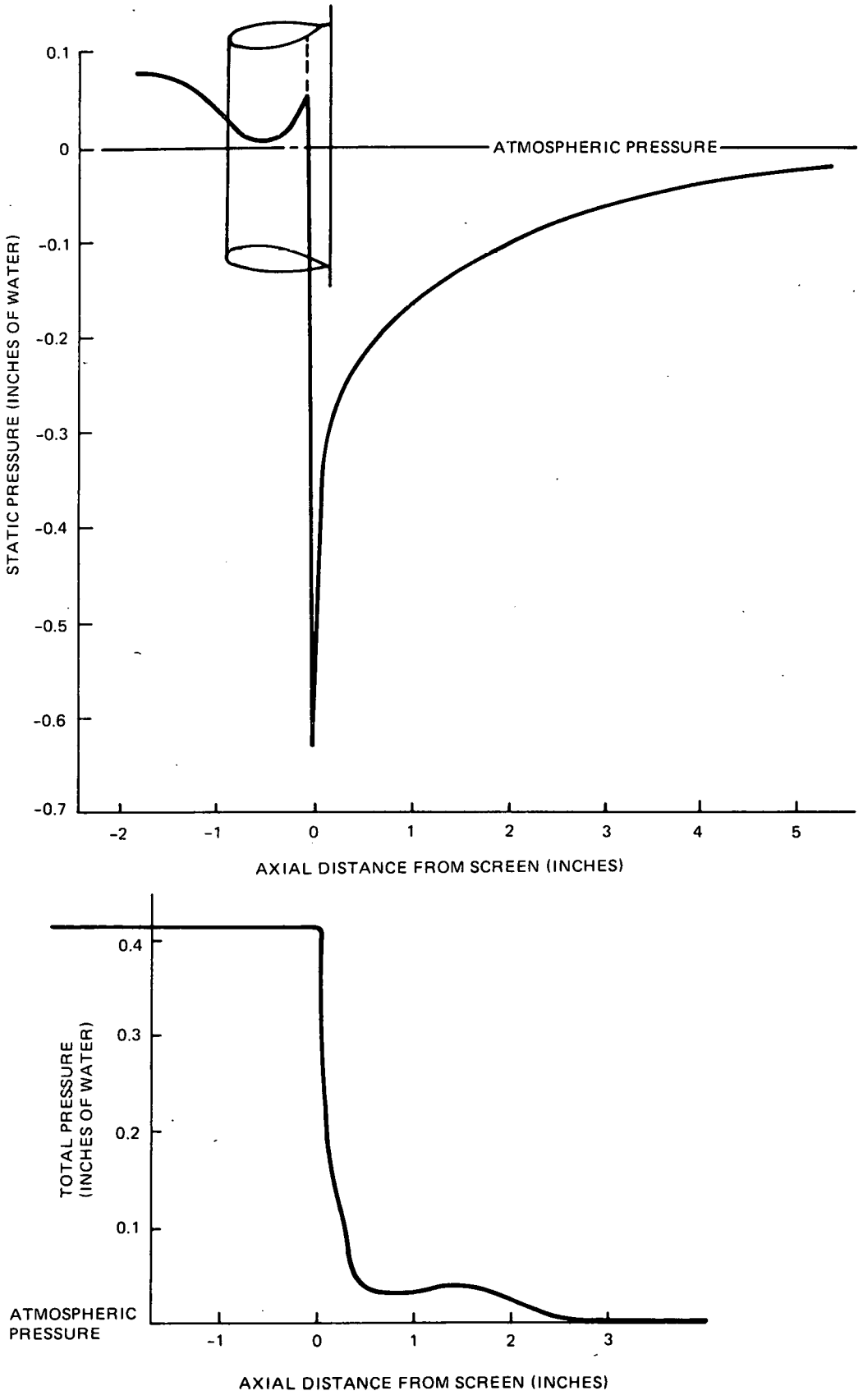

Figure 19 Typical Centerline Axial Static and Total Pressure Surveys of a Flapped Williams "A" Contour Ring Wing Diffuser, $C_T = 0.89$

coefficient, C_{p_4}, of -0.54. Full recovery to atmospheric pressure by mixing of the free jet with the surrounding air flow takes place at downstream distances greater than about 10 diffuser chord lengths. The centerline augmentation ratio, r, calculated by the method previously described, is 1.3 for this model and disk loading.

The total pressure and static pressure traces of Fig. 19 are analyzed like those of Fig. 18. The disk loading for this flapped Williams A configuration is 0.89 q_o with the screen simulator mounted at the 80 percent chord location. The local dynamic pressure, q_2 = 0.87 q_o and the diffuser exit plane pressure coefficient, C_{p_4} = -0.64. The relatively more subatmospheric diffuser pressure, compared to the performance shown in Fig. 18, results in a greater centerline augmentation ratio value of 1.40.

For both the flapped NACA 4412 and Williams A contour diffuser configurations, it is found that more rearward positioning of the simulated turbine yields higher performance than if it were located near the leading edge, at the minimum cross section, or within $\pm$5 percent chord (c) of the trailing edge of the diffuser. For example, comparative data for a diffuser documented by Fig. 18 but with the turbine simulator at about 75 percent c, instead of 10 percent c, yields a greater centerline r of 1.6 and a q_2 of 0.94 q_o at the same value of 0.83 q_2 disk loading.

The variation of augmentation ratio, r, with turbine loading, C_T, is shown in Fig. 20 for ring wing model configurations (1b) and (2b) (refer to Table 5). Also spotted are data points for models (1a), (1c), and (2a), each at a single disk loading value. The general trend of increasing augmentation ratio with

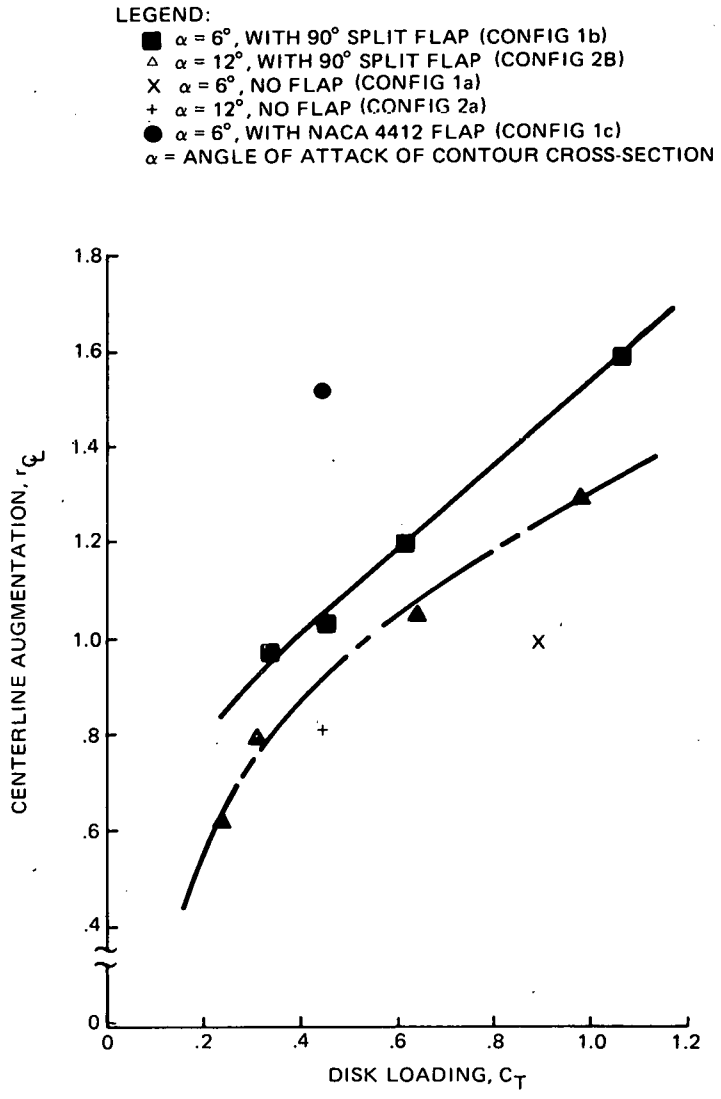

Figure 20 Centerline Augmentation of NACA 4412 Contour Ring Wing Diffuser Configurations at Different Disk Loadings

C_T up to loadings of 1.06 is evident from these test data. The diffusers equipped with split flaps show augmentation ratios that are 45 percent (for model 1) and 20 percent (for model 2) greater than the basic diffuser. The airfoil flap-equipped ring wing (model 1c) has 88 percent better performance than the basic airfoil design, and is approximately 50 percent better than the split flap equipped diffuser. Normally, the wing section lift coefficient, C_L, increases with angle of attack, α, until stall angle is reached. For the NACA 4412 section, $\alpha = 16°$ is the stall angle. From this characteristic behavior one would expect the diffuser for $\alpha = 12°$ (i.e., model 2) to perform better than for $\alpha = 6°$ (i.e., model 1). However, the reverse trend is seen to exist by our data for split flap equipped diffusers. The reason is the flap type of lift improvement device shifts the stall angle to $\alpha = 11°$, and the C_L drops very rapidly with further increase in α (Ref. 11). The superiority of the airfoil-shaped flap over the split flap as a lift augmentation device is confirmed by our data. However on the basis of cursory consideration of fabrication complexity, wetted surface, and bulk, the split flap technique appears to be more cost effective than the two-airfoil element.

Our tests indicate a design approach that links the contour exhibiting the highest attainable section lift coefficient with the best attained ring wing diffuser performance. There is reason to expect (e.g., see Igra report, Ref. 2) that augmentation does not increase indefinitely with disk loading. However, within the range of turbine-simulating screens available during this contract period we were unable to observe a peaking value or trend. Further work along this direction is planned in future activities.

Values of the ratio of turbine approach velocity to free stream velocity $(q_2/q_o)^{\frac{1}{2}}$ are given in Fig. 21 for the NACA 4412 contour

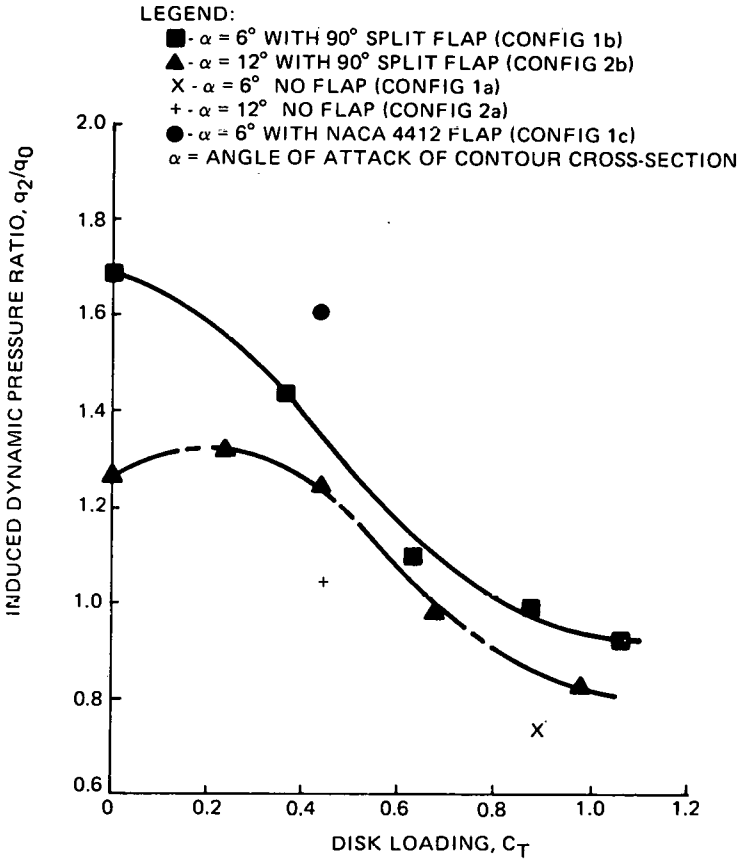

Figure 21 Centerline Induced Dynamic Pressure Ratio for NACA 4412 Contour Ring Wing Diffuser Configurations at Different Disk Loadings

diffusers. The general trend may be summarized as varying from values greater than 1.0 at low to moderate turbine disk loadings to slightly less than 1.0 at C_T above 0.7 to 0.8. Theoretical predictions for the optimum actuator disk give a ratio of velocities of 67 percent. It is therefore apparent that the diffuser induces higher mass flows through the turbine than for the optimum unshrouded configuration. It is possible to relate, then, the augmentation rato of any turbine mounted in a particular diffuser design to its measured (q_2/q_o) value in an unambiguous way, from such data as given by Figs. 20 and 21.

Such lack of ambiguity is not possible solely by measurement of the diffuser exit pressure. The curves of C_{p_4} given in Fig. 22 for the two short length NACA 4412 designs show that the values, between -0.60 and -0.70, are all comparable to the best designs of longer diffusers reported by Igra (Ref. 2) and could not have been predicted a priori.

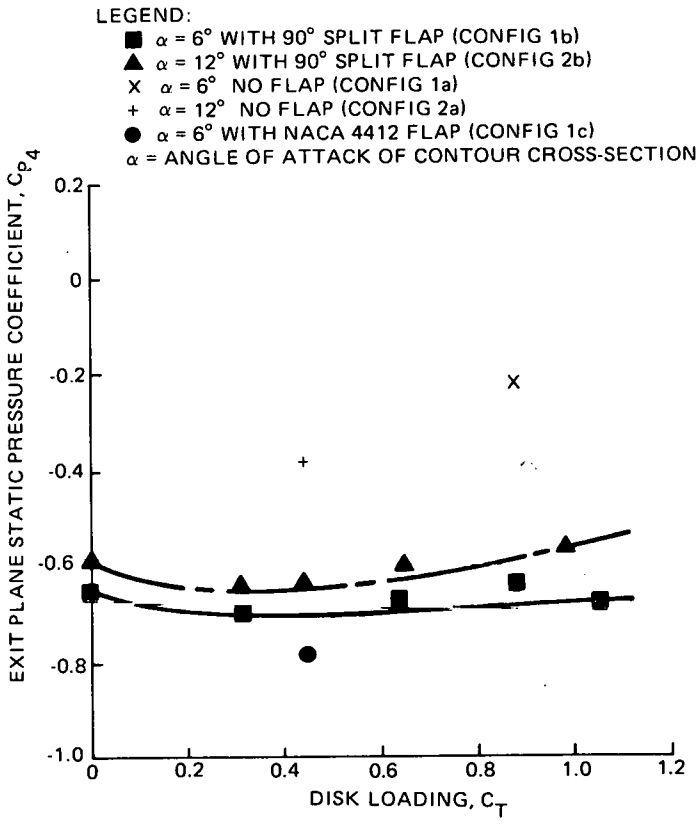

Figure 22 Exit Plane Pressure Reduction for NACA 4412 Contour Ring Wing Diffuser Configurations at Different Disk Loadings

Figure 23 shows the variation of augmentation ratio with turbine loading for the Williams A type airfoil ring wing diffusers and for one test with the Liebeck airfoil contour. Although the trend for the Williams A design is similar to that for the NACA 4412, the r levels are slightly higher for the latter configuration fitted with 0.20 split flap. The use of a split flap instead of an airfoil shaped flap with the Williams airfoil does not

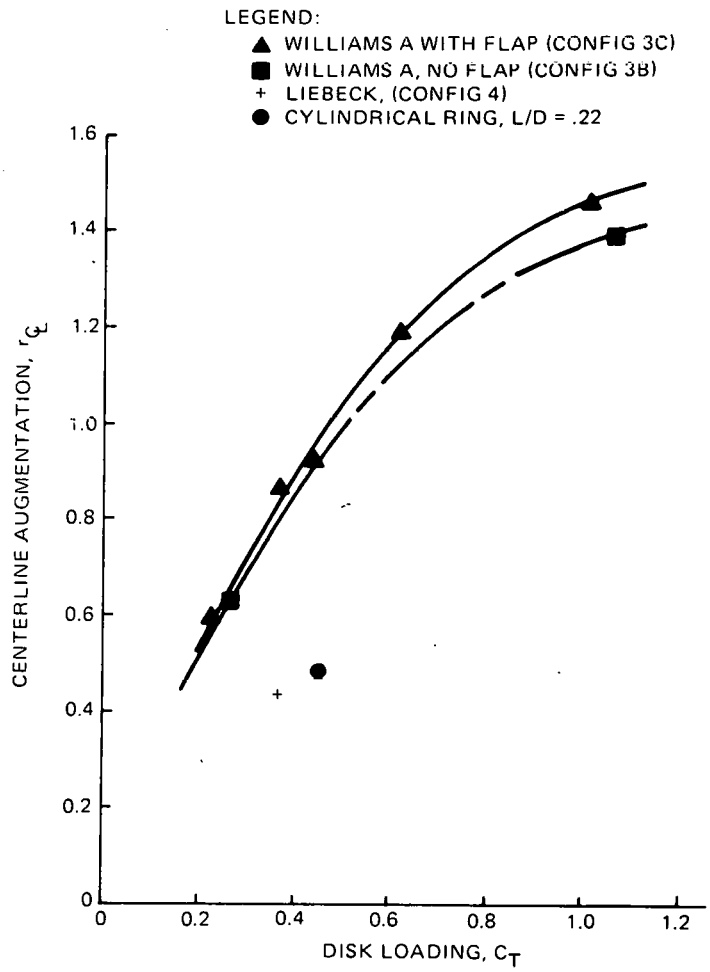

Figure 23 Centerline Augmentation for Williams "A" and Liebeck Contour Ring Wing Diffusers at Different Disk Loadings

produce the dramatically higher augmentation performance found in the NACA 4412 design. Although the theoretical lift coefficient of the Williams shape is larger than the NACA 4412 and should produce greater augmentation, the test results did not show this. Some reasons for this result include the possibility that the model template did not reproduce the Williams contour with sufficient precision and that we used too small a model size (i.e., Reynolds number effects) to obtain full realization of the theoretical section lift. The short axial length of the main Williams contour, however, warrants further examination of this approach, possibly

at $\alpha > 0°$, in contrast to $\alpha = 0°$ employed for the models of the reported test series.

The results of the Liebeck contour diffuser at the one low disk loading tested are disappointing. Even though this supposedly high lift design may yet prove to be of superior performance at high turbine loadings, the inherently more massive and weighty characteristics of this basic shape give it a low priority in our application. A simple short cylindrical tube appears to offer as much aerodynamic benefit, albeit poor, as the Liebeck contour ring wing diffuser.

The data on ratio of local to free stream dynamic pressure, q_2/q_o, are given by Fig. 24 for the range of disk loadings tested. All models and test conditions appear to yield greater mass throughput for the simulated turbine than a best unshrouded turbine. The diffuser exit plane pressure, represented by the coefficient C_{p_4}, is highly subatmospheric for all ring wings and scattered about a mean value of about -0.60. The split flap equipped Williams contour yielded the greatest measured suction pressure, -0.82 q_o, at a relatively low turbine loading. However, the low loading more than offset the enhanced mass flow to produce an augmentation ratio that was only about 0.60. The simple short cylindrical ring produces an exit plane pressure very close to atmospheric, and holds no promise as an augmentation device.

In summary, the aerodynamic performance of short flapped ring wing diffusers, with NACA 4412 and Williams A contours, yields appreciable power augmentation of highly loaded wind turbines. The limiting potential of this augmentation has not yet been reached at a turbine disk loading approaching slightly greater than 1.0 q_2.

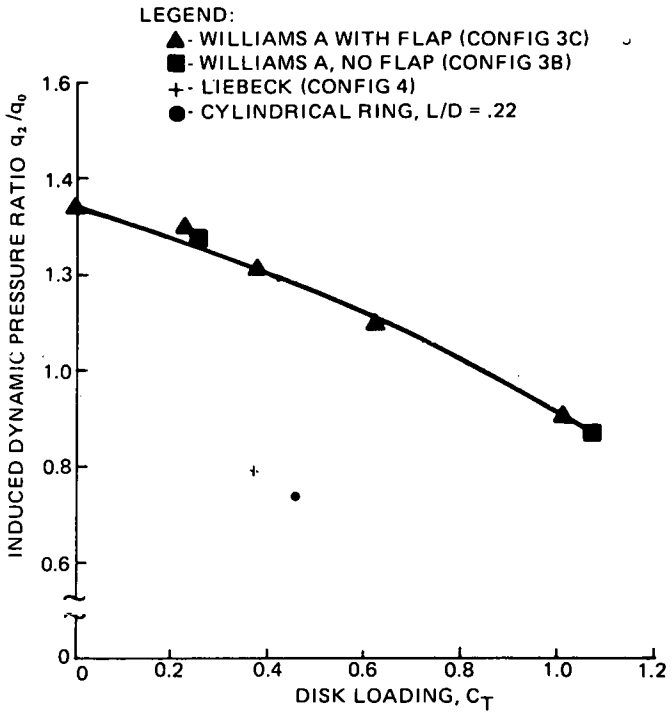

Figure 24 Centerline Induced Dynamic Pressure Ratio for Williams "A" and Liebeck Contour Ring Wing Diffusers at Different Disk Loadings

ANALYSIS OF FLOW THROUGH DIFFUSERS BY METHOD OF SINGULARITIES

The inviscid flow about an axisymmetric conical diffuser can be calculated using the so-called method of singularities. This general approach to the problem has been discussed by Küchemann and Weber (Ref. 12). In particular, for a thin walled annular diffuser, an appropriate distribution of ring vortices can be combined with a uniform flow along the axis to yield the desired flow. The distribution of vorticity along the diffuser surface must be such as to satisfy the condition of zero normal velocity at the diffuser surface and must also satisfy the Kutta condition of no velocity discontinuity at the diffuser trailing edge.

The calculated pressure at the exit plane is in all cases for a 10 vortex ring solution less than atmospheric pressure p_o.

From Bernoulli's equation we would expect the velocity over the exit plane to be greater than V_o, i.e., there is an enhanced flow through the diffuser exit plane over what would occur in the absence of the diffuser. This increase in flow is strictly an inviscid flow effect and is really caused by the lift forces of the diffuser wall on the fluid which result in additional fluid being directed inward and through the diffuser.

This effect may be understood more easily by examination of the flow streamlines plotted in Fig. 25, where the upper half of a vertical section through the diffuser centerline is shown. The centerline flow is represented by the abscissa axis, and the flow

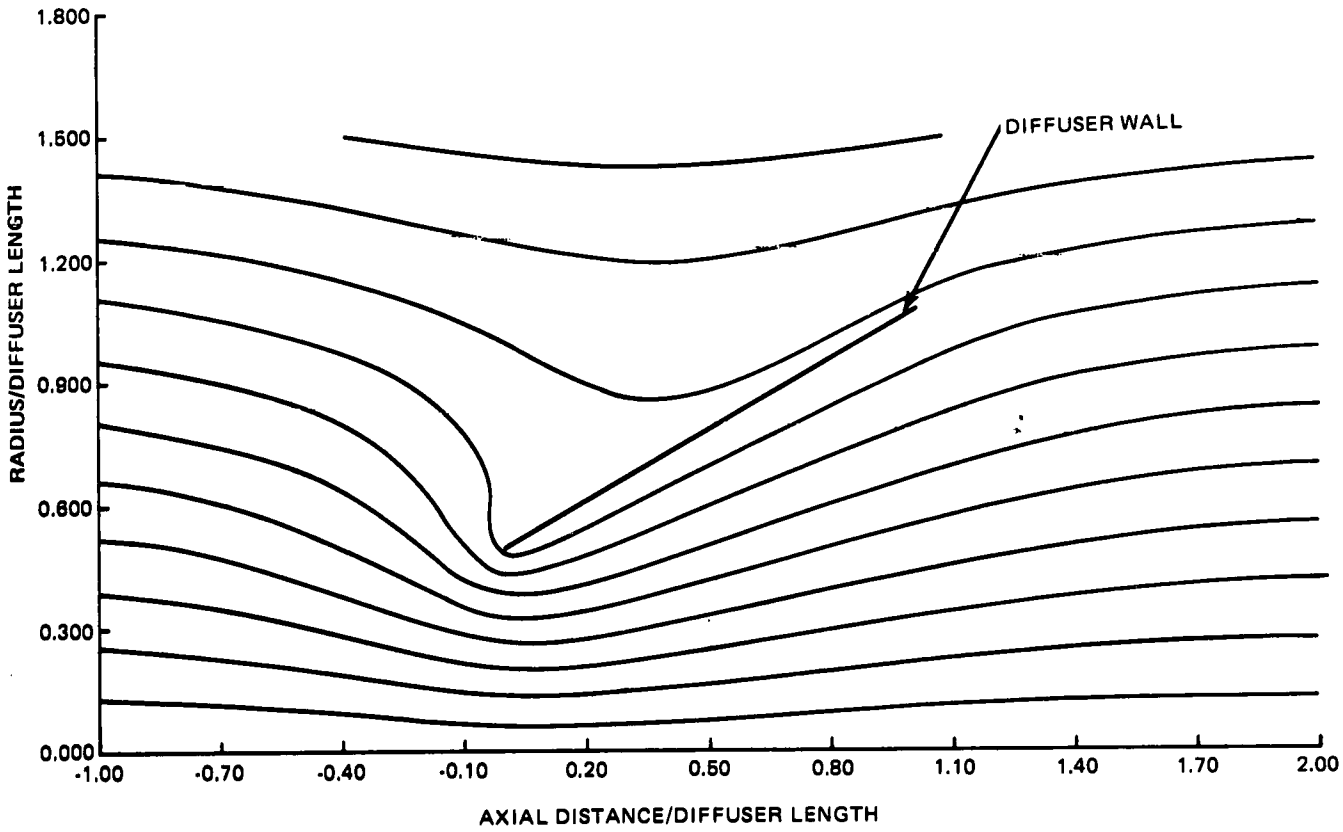

Figure 25 Streamlines Computed by the Method of Singularities for a 30° Half Angle Diffuser

at the upstream and downstream ends of the plot are seen to approach roughly uniform flow. The convergence of the upstream flow into the diffuser, resulting in an increased flow, is easily observed. Likewise a continued expansion of the flow (pressure recovery) downstream of the diffuser exit can be noted.

The present analysis assumes no separation of the flow — this condition is realized in the experiment by use of slots. Also since the analysis is inviscid, boundary layers are neglected — this is probably not a bad assumption since the actual boundary layers may be relatively thin due to the use of blowing through slots. A more serious error is neglecting the wind turbine at the diffuser entrance. This shortcoming can be partly overcome, however, by an extension of the method of singularities, and this part of the analysis is currently being done. The extension involves superimposing on the flow through the diffuser a reverse flow caused by a series of vortex rings (rotating in the opposite sense to those considered previously) located along the wake stream surface. The vortex strengths along the diffuser surface must be readjusted to maintain zero normal velocity at the diffuser surface. The vortices along the wake are chosen to be of such a strength that the resultant decrease in flow through the diffuser is equal to that caused by the flow resistance of the wind turbine. By further refining the method of singularities it is possible to account for the presence of slots in the diffuser wall, a finite gap between the diffuser inlet and the outer edge of the wind turbine, and effects of finite wall thickness. We can also compute the effects of nonuniform flow over the turbine disk.

3. ECONOMIC ANALYSIS

GENERAL CONSIDERATIONS

Economic assessment of the diffuser-augmented wind turbine (DAWT) relative to a conventional wind energy conversion system (WECS) requires that the most competitive versions of each concept be identified, their performance measured, and then priced according to consistent costing rules. Identifying the cost-optimized DAWT is more complicated than for conventional WECS, because there are more parameters affecting the economics and there is a paucity of good performance and costing laws for very large diameter, short diffusers.

Our goal is to compare capital cost per unit power produced over an annual wind spectrum, so we must identify the DAWT that has the best value of that parameter, and compare its value to that of the best conventional WECS. We have found the graphical portrayal of Fig. 26 to be useful in understanding this process, and relating it to standard treatments by economists. In Fig. 26, the curves are sections of constant augmentation ratio through the surface that represents the locus of best achievable DAWTs (from a cost standpoint) for various power levels. With $r = 1$, we have a conventional WECS.

Along any constant r curve, for a particular design concept of wind power conversion systems, the average cost of unit production capacity first decreases as the power level of the unit increases due to the usual economics of scale. At some power level, any further increase in unit capacity requires an extension of rotor diameter past the aeroelastic limits for low cost construction that results in an increased average cost for the power. In economic analyses the minimum average cost is found always at the

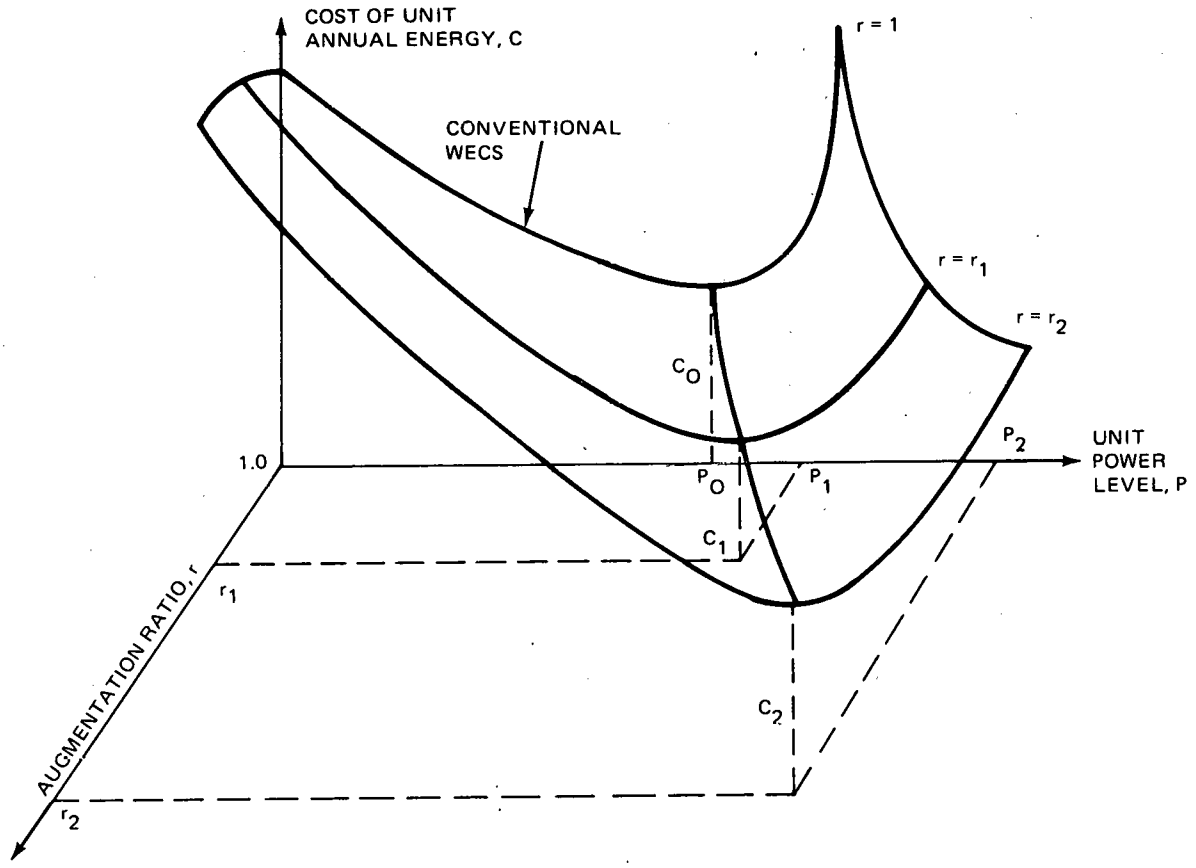

Figure 26 Surface of Lowest Cost Designs for Comparison of DAWT to Conventional WECS

output that makes optimum use of capital. This occurs where the incremental cost needed to add the last increment of output just equals the average cost of total production. In mathematical terms, to optimize the cost of wind power production we need $C = C'$ where

$$C \equiv \frac{1}{P}\int_0^P C'(x)dx \quad , \quad \text{the cost of unit annual energy}$$

where

$$C' \equiv \frac{\partial(PC)}{\partial P} = \frac{\partial C}{\partial P} + C \quad , \quad \text{the incremental cost}$$

The equality $C' = C$ exists when $\partial C/\partial P = 0$. This establishes the criterion for minimum C in a plane of constant r.

Changing the design concept of a wind power conversion system by adding augmentation, creates a new curve describing the variation of cost with power level at a new (constant) r. This new curve will have a different minimum cost point which may or may not be less than the previous curve's minimum. The problem then becomes to establish that a design point $C_1(r_1,P_1)$ exists, where $C_1 < C_o$, and to determine the particular $C_1(r_1,P_1)$ at which the cost of unit annual energy is the absolute minimum for the entire surface of lowest cost designs.

Even after identifying the most cost effective design point C_1, many applications may exist that require construction at off-optimum conditions. When construction of a unit at this design point results in the generation of more power than is required, an uneconomic allocation of material resources and capital results. On the other hand, insufficient power generation capacity with respect to actual future demands can reduce economic incentives for growth. The most economical system power capacity is usually one rated at slightly more than the current expected demand level.

COST ESTIMATES

Diffuser

In the course of investigating the economics of DAWT utilization, it became evident that no meaningful results would be forthcoming without a stress analysis, at least at the preliminary design level. Once the structure was defined, the associated costs could be estimated. A diffuser configuration was selected as a baseline design, with the understanding that any of its features

may change. The configuration selected for stress analysis was a 30° half angle (θ), boundary layer control diffuser design for a turbine diameter of 60 meters; this baseline design gives an average augmentation ratio of 1.89 in our model tests.

The design analysis applied here combines shell theory with use of a computerized finite element structural analysis. The design criteria are

- The material yield strength must not be exceeded
- The radial deflection of a ring section around the turbine position shall not exceed 1.5 percent of the radius

The latter specification prevents the turbine from striking the diffuser wall and is in a range of tip clearance ($\frac{1}{2}$ to 3 percent radius) that gives good ducted turbine performance (Ref. 13).

The maximum wind speed for an operable turbine is taken at 75 mph. Although the turbine will be feathered or braked at higher speeds, the diffuser wall must be capable of withstanding winds having dynamic pressures up to 60 psf, corresponding to 150 mph at sea level (Ref. 14). In the most extreme wind speed case, a project lifetime risk of occurrence of 3 percent or less (Ref. 15), provisions for supplementary tie-down cables are assumed, and the deflection criterion is abandoned. The tied down, 150 mph wind condition leads to more severe stresses in the diffuser structure than the 75 mph maximum turbine operable condition.

The large full scale diffuser structure can best meet the design criteria by use of a double wall construction consisting of relatively thin surface plates, or skins, separated by rings of depth, h. This type of structure is primarily subjected to bending loads. The diffuser assembly assumed for the baseline design

is to be supported by two rigid structures running the entire length of the diffuser and circumferentially offset by 20° from the keel line of the diffuser (see Fig. 27). These supports are on a rotating platform to accommodate movement of the DAWT into the active wind direction. Other support options will also be examined in future designs. The total structure then consists of the skins, rings, and support truss. In a practical sense, the total ring weight is a fixed percentage between 10 and 15 percent of the diffuser skin weight.

The weight of the diffuser structural material based on both the strength and radial deflection criteria is given by

$$W = \frac{C(\delta^*/R_2)(q_s^2/q_d)(E/\rho)\ell R_2^2}{(\sigma_y/\rho)^2\,[1 + (h_4/h_2)]^2}\left[1 + \left(\frac{\ell}{R_2}\right)\frac{\sin\theta}{2}\right]^5$$

where

C = proportionality constant

δ^* = allowable deflection

R_2 = turbine radius

q_s = dynamic wind pressure for yield criteria (at 150 mph)

q_d = dynamic wind pressure for deflection criteria (at 75 mph)

E = modulus of elasticity of diffuser material

ρ = diffuser material density

ℓ = running (slant) length of diffuser shell

σ_y = yield strength of diffuser wall material

h = depth of wall structure of the diffuser

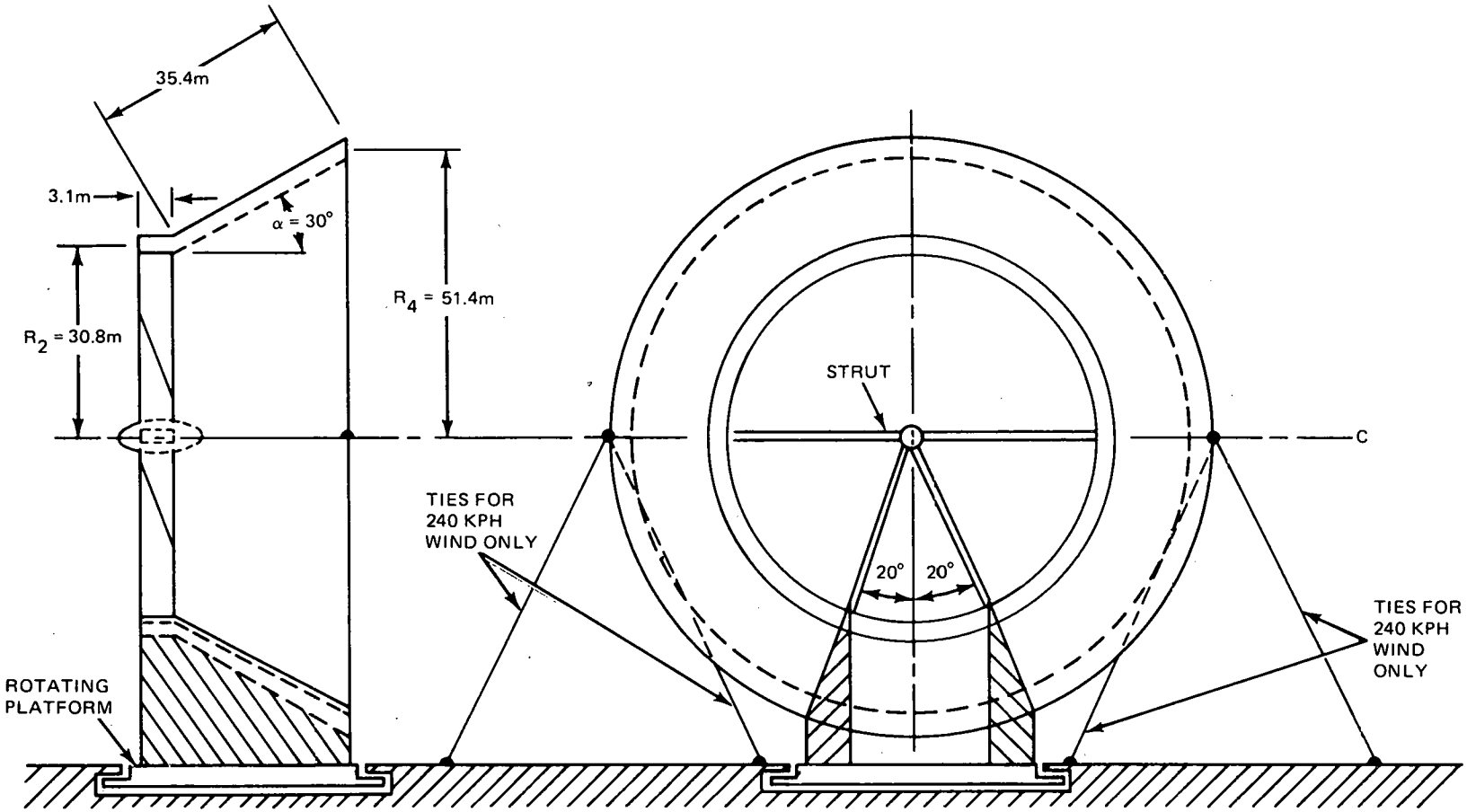

Figure 27 Diffuser Baseline Design

The total material cost of the diffuser is the unit cost U_c of the structural material used, $/pound, times the total weight, or $U_c \times W$. For a particular diffuser and turbine design, yielding an augmented power of rP, where $P \propto D_1^2$ at a constant wind speed, the average material cost, AMC, of the diffuser structure above is $(U_c \times W)/D_1^2 = AMC$, and the AMC per unit power is $AMPC = AMC/r$.

For different materials of construction the diffuser AMC is proportional to $(E\rho/\sigma_y^2) \times U_c$. A relative AMC comparison of some common fabrication metals is listed in Table 6 for current prices in mill quantities of structural material (Ref. 16).

TABLE 6 RELATIVE COSTS OF MATERIAL OF CONSTRUCTION FOR WIND TURBINE DIFFUSERS

Type/ Material	E, psi	ρ, lb/in.^{3}	σ_y, psi	U_c, $/lb	Relative AMC
HSLA Steel	30×10^6	0.282	120,000	0.14	1.00
HSLA Steel	"	"	80,000	0.13	2.09
HSLA Steel	"	"	16,000	0.12	6.46
6061 Alum.	10.5×10^6	0.10	40,000	0.85	6.46

Our baseline selection of high strength, low alloy (HSLA) constructional plate steel for diffuser construction is easily fabricated by standard welding and fastening techniques and is the preferred material for pressure vessels, tanks, offshore platforms, and heavy duty mining and earth moving equipment. Maintenance for such material is minimal because of its inherent corrosion resistance properties. Much higher strength steels (i.e., super alloys)

are also feasible, but at a greatly increased price and with less availability and familiarity among fabricators. As compared to steel, the much higher price per pound of commercially available aluminum alloys and their lower yield strength offset their lower weight, elasticity modulus, and corrosion resistance. Very high strength aluminum alloys are very costly and will not radically change aluminum's unfavorable competitive position. As indicated in Table 6, a steel diffuser equal in cost to aluminum would require relatively low yield strength alloys compared to steels with material properties currently considered readily available. While aluminum is attractive from a maintenance and aesthetic viewpoint, its comparatively higher average cost (see Table 6) precludes its further consideration for wind turbine diffusers.

The average total cost, ATC, of the fabricated diffuser is estimated from the statistical relationship of total sales to material cost for typically similar industries. By using U.S. Department of Commerce data, presently available only for the period 1969-1971, for several appropriate industries (see Table 7; also Ref. 17), we have applied a factor of 2.2 for full scale diffusers. It is reasonable to assume that such a structure could have major prefabrication in highly industrialized regions of the U.S. and then be shipped as knocked-down components to the ultimate assembly site for use. Our "factored" cost estimate probably is accurate to ± 10 percent of the actual cost of full scale production.

The variation of diffuser total average cost, $\bar{\$}$, with turbine diameter, D_2, for geometrically similar designs is

$$\bar{\$} \propto L\left(1 + \frac{L}{D_2} \sin \theta\right)^5$$

where L is the axial length, if governed by both deflection and strength criteria. But, for the fixed dimensional relationship of

TABLE 7 1969-1971 INDUSTRY-WIDE FACTORS OF (SALES/MATERIAL COST)

SIC Code	Industry	Average Factor
33	Primary Metal Industry	1.70
34	Fabricated Metal Products	2.1
3441	Fabricated Structural Steel	1.85
3444	Sheet Metal Work	2.0
3446	Architectural Metal Work	2.25
3567	Industrial Furnaces and Ovens	2.0
37	Transportation Equipment	1.70
3721	Aircraft	2.3
3731	Ship Building	2.3

L/D_2 = constant recommended by model test results, we obtain for the diffuser

$$\bar{\$} \propto D_2$$

However, as the turbine diameter decreases the deflection criteria can be relaxed somewhat because absolute deflections will approach the order of magnitude of construction dimensional accuracy. Under these conditions, the specific strength criterion probably becomes controlling. The diffuser weight varies with D^3L for this criterion, and $\bar{\$}$ varies as D^2. Accordingly, to account for some tendency of diffuser weight to vary nonlinearly with diameter as size decreases, we estimate the average variation as being proportional to the 1.25 power of turbine diameter between 10 and 60 meters, or $\bar{\$} \propto D_2^{1.25}$. For diameters greater than 60 meters, both structural criteria must be satisfied rigorously, and $\bar{\$} \propto D$ is assumed to hold.

The total weight of a diffuser for a 61 km (200 ft) diameter turbine is estimated at less than 500,000 kg (1,100,000 pounds) when constructed of HSLA steel. The fabricated diffuser should cost

a total of about $335,000, resulting in diffuser $\bar{\$}$ (i.e., dividing by D^2) of approximately 90 $\$/m^2$; the average cost per unit power, ATPC, is about 47 $\$/m^2$. By comparison, one recent authoritative estimate (Ref. 18) for the weight of a 61 km diameter turbine made of composite material is 18,180 kg (40,000 pounds), costing $400,000, and resulting in a wind turbine $\bar{\$}$ of 107 $\$/m^2$.

Rotor

The large wind turbine project, initiated by NASA-Lewis Research Center as part of the ERDA program, has made possible an updated detailed examination of wind turbine costs (Refs. 18 and 19) in the 100 to 1500 kW rated power range. The estimated costs for production quantities (i.e., $\sim$ 100/year or greater) also have been summarized recently (Ref. 20) for Mod-1 designs. Based on this authoritative information, we have synthesized the trend of average rotor costs with diameter.

The traditional curve representing average cost versus size (or quantity) is U-shaped, and described by an equation of the form $y = k_1 e^{x} + k_2 e^{-x}$. Modern economics theory explains this shape as the result of initial economics of size (i.e., bulk transactions, massed reserves, and specialization) that produce lower average costs as size increases. However, beyond a certain size or quantity, the sources of initial economy no longer remain available and further increments of size become relatively more costly. The change of conditions, producing an increased average cost trend, creates the over-all U-shape.

The normal curve up turn in average cost for larger units than can be produced optimally is accentuated further in the case of wind turbines by the problems of aeroelastic stresses in large cantilevered structures. The major stresses on a blade hub design arise from centrifugal radial tension and thrust bending moment. It can

be shown that the total stress σ_T, combines the effects of the two forces and equals

$$\sigma_T \sim \frac{\bar{c} R^2 \Omega^2}{C_h^2} \left(1 + \frac{R^2}{C_h}\right)$$

where

$\bar{c}$ = average blade chord

Ω = rotational speed

C_h = effective diameter of blade hub section

R = blade radius

For constant Ω, blade aerodynamic characteristics, and blade solidity ($\sim \bar{c}/R$), the hub stress is proportional to a high power of blade radius

$$\sigma_T \propto R^4 \quad \text{since} \quad R >> C_h$$

Then, the turbine blades can be made geometrically similar for different sizes only when the total stress σ_T is equal or less than the fatigue strength, σ_f, of the blade material. For larger rotor sizes, extraordinary design measures must be exercised and turbine costs can no longer be extrapolated on the basis of smaller turbine costs. At present, it is reasonable to consider turbine rotor diameters up to about 65 meters ($\sim$ 210 ft) as being within current capabilities to design and manufacture reliably operating turbines. For rated systems requiring much larger diameter blades, current practice suggests secondary support trusses or replicative assemblies of smaller turbines on a common support superstructure at a common land site.

The Kaman Aerospace Corporation cost estimates for advanced composite turbine blades are approximately 67 $\$/m^2$ for the 500 kW rated system (diameter = 45.7 meters) and 92.6 $\$/m^2$ for the 1500 kW rated system (diameter = 54.8 meters) (Ref. 19). The

Kaman turbine cost trend between 45 and 75 meters diameter follows a relation of (Ref. 17)

$$\$ = 4440\ e^{0.023D}$$

where D is in meters. The average cost is then described by

$$\overline{\$} = \frac{4440\ e^{0.023D}}{D^2} \quad , \quad \$/m^2$$

The General Electric Company estimates, published about midway in their contract period (Ref. 22), presented a cost trend between 20 and 100 meters diameter described by

$$\$ = 33.77\ D^{2.22} + 20{,}000$$

Later, at the conclusion of their contract GE had revised the rotor costs to 75.5 $\$/m^2$ for the 500 kW rated system (diameter = 55.8 meters) and 84.4 $\$/m^2$ for the 1500 kW rated system (diameter = 57.9 meters) (Ref. 19). This final design study gives a cost relation of $\$ = 1732 \exp(0.088\ D)$ and an average cost of

$$\overline{\$} = \frac{1732\ e^{0.088\ D}}{D^2} \quad , \quad \$/m^2$$

The results of these estimated average rotor costs for both study organizations and Grumman's estimate of diffuser (only) average cost are given by Fig. 28 between 10 and 100 meter rotor diameters. Examination of this figure reveals that

a. There is a large variation in turbine cost estimates for small to moderate size rotors, depending on the organization conducting the analysis

b. Both turbine design teams have optimized the cost of their configuration at around 25 meters diameter

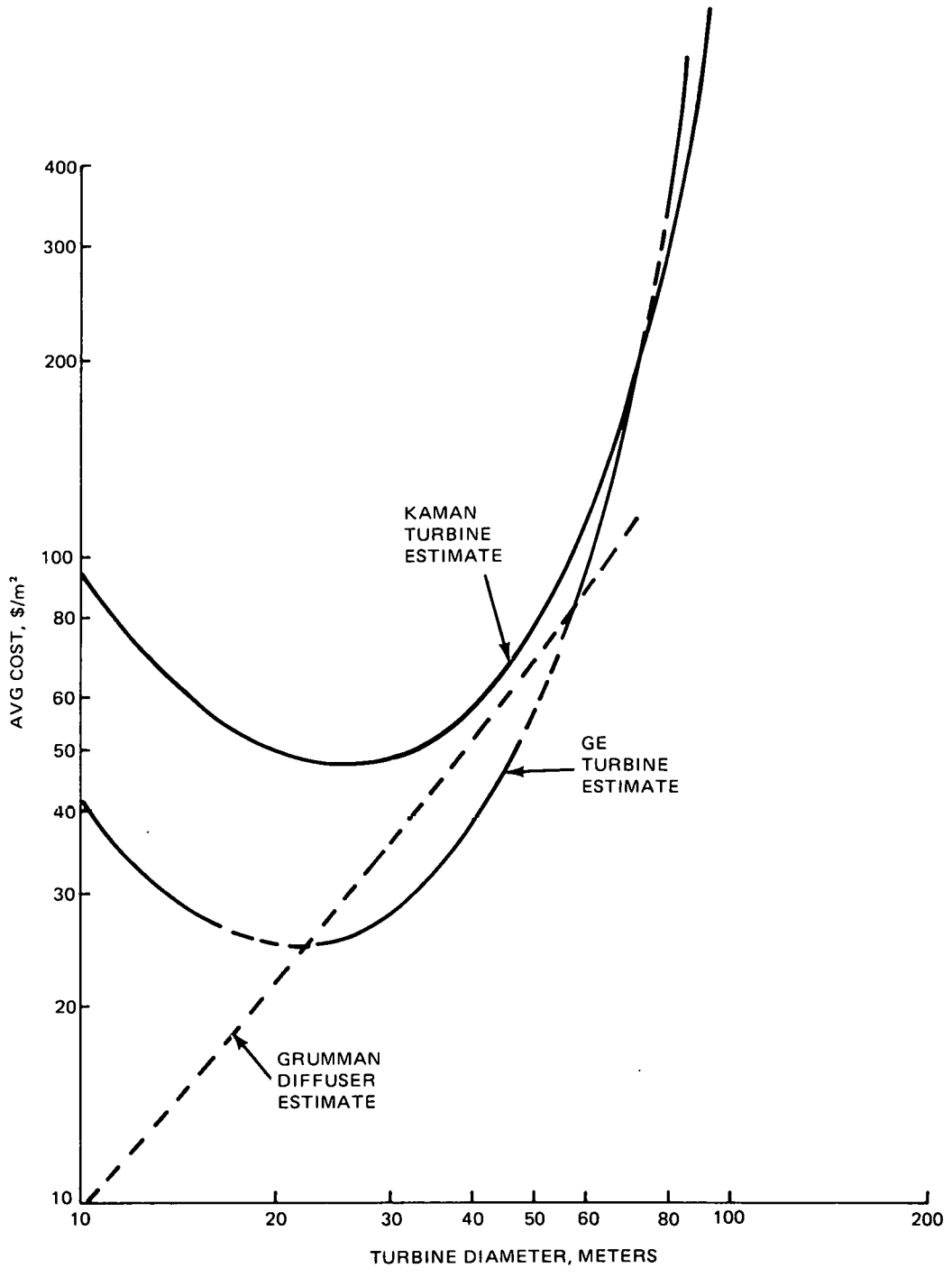

Figure 28 Average Cost Estimates of Wind Turbine Rotors and a Baseline Diffuser Component

c. The difference in estimated average cost for very large diameter rotors (i.e., above 60 meters) is negligibly small between both design groups. This fact may arise from the relative inexperience of the entire engineering profession in construction of such large diameter turbines which forces independent designers into similar designs based on the best consensus practices

d. Between about 25 and 55 meter diameters, the average cost of the diffuser is within the range of the two rotor estimates. However, initially the average cost of the rotors decreases with size while the diffuser average cost increases. Only beyond about 45 meters does the rate of increase of diffuser average cost become less than that for the turbine.

With this present band of uncertainty clouding most of the rotor cost estimates, there probably can be no clear cut economic conclusion except to state that diffuser costs are no greater than rotor costs, and can be much less. Further, since diffusers are not subject to cyclic centrifugal stresses, the average cost of diffusers for very large diameter turbines is always going to be less than for the rotor itself.

WIND UTILIZATION FACTOR

Because of wind turbine operational problems, the full annual spectrum of wind speeds, or the total annual wind energy, cannot be utilized. One of these turbine limitations is the maximum velocity that can be sustained before structural damage occurs to the turbine blades. For higher wind speeds, the turbine must be feathered or braked so that the converted wind power is essentially zero. Another

limitation is the minimum wind speed needed to produce enough turbine torque to overcome bearing friction and windage losses, and meet speed control criteria of the power generation system. Between the minimum and rated wind speeds the turbine performance and control system logic restricts the output power to a level less than the rated value. The yearly usable output of the wind turbine then is some factor of the total annual wind energy potential which is called the "usable energy pattern factor," k_{eu}, defined as

$$k_{eu} = \frac{V_R^3(t_2 - t_1) + \int_{t_2}^{t_3} v^3 \, dt}{8760\left[\frac{\int_o^t v \, dt}{8760}\right]^3}$$

where

V_R = rated wind speed

v = instantaneous (short term) wind speed

t_1 = hours of year when maximum wind speed is exceeded

t_2 = hours of year when rated wind speed is exceeded

t_3 = hours of year when minimum wind speed is exceeded

For conventional optimum WECS, the local air speed at the leading edge of the turbine blades theoretically is 2/3 of the free wind speed. The minimum wind speed, V_{o_c}, would be reduced by 1/3 at the WECS optimum turbine; or $V_{t_c} = (2/3)\, V_{o_c}$. However, for DAWTs the ratio $V_t/V_o = \epsilon$ is greater than 2/3 because of the preturbine acceleration produced by the diffuser. Then for the same cut-in torque power, the DAWTs turbine can operate at a lower free wind speed than the WECS, or

$$(V_{o_c})_{DAWT} = \frac{(2/3)}{\epsilon} (V_{o_c})_{WECS}$$

This characteristic permits DAWT to operate over annual periods, t_4, much larger than for WECS. The diffuser produced speedup upstream of the turbine can be accounted for in designing the turbine at rated output, so that the same rated wind speed, V_R, can be associated with both DAWT and WECS. Because the DAWT operates at a lower turbine loading than WECS (typically peak C_T of 0.6 compared to WECS optimum loadings of 2.0) the DAWT can operate at maximum wind speeds equal to WECS despite the diffuser speedup of the former system. For these reasons, DAWT can operate at rated output over the same $(t_2 - t_1)$ annual time interval as WECS, if so desired.

The significance of this brief discussion is that the k_{eu} factor for DAWT can be larger than for WECS because

$$K_{eu} \equiv \frac{(k_{eu})_{DAWT}}{(k_{eu})_{WECS}} = \frac{V_R^3(t_2 - t_1) + \int_{t_2}^{t_3} v^3 dt + \int_{t_3}^{t_4} v^3 dt}{V_R^3(t_2 - t_1) + \int_{t_2}^{t_3} v^3 dt} > 1$$

since $t_4 > t_3$.

Figure 29 shows typical annual frequency distributions of wind velocity in potentially attractive mountainous and off shore installation regions (Ref. 23). Between occurrence frequencies of 0.3 and 0.9, these curves can be approximated by a linear expression

$$v = at + b$$

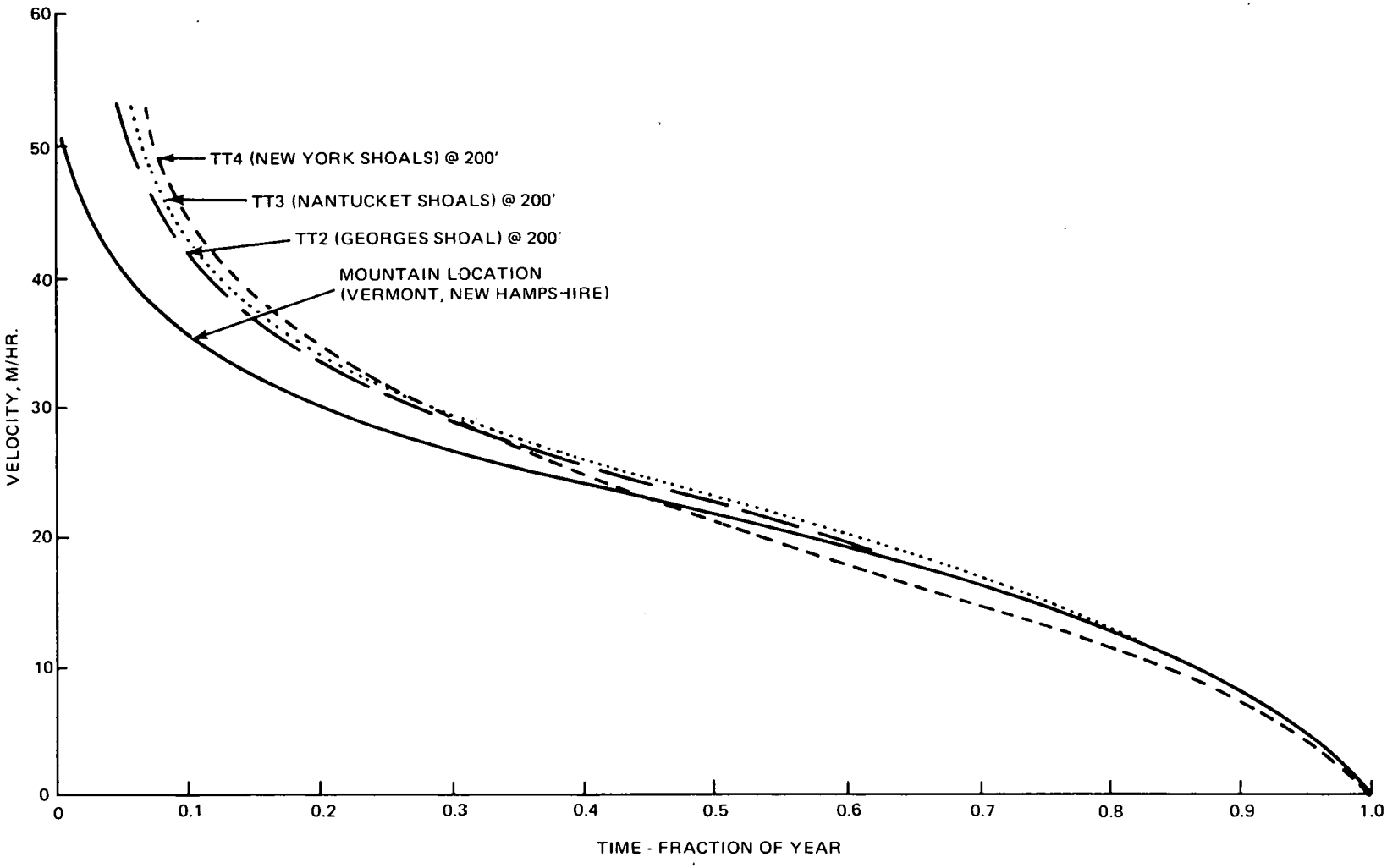

Figure 29 Typical Annual Frequency Distribution of Wind Velocity in Potential Installation Regions (Ref. 23)

where $a = -0.0037$ and $b = 38.25$ for trends of Fig. 29. Then, approximately, $(t_4 - t_3) = [(2/3)/\epsilon - 1](t_3 + b/a)$ and the additional usable power for the DAWT is approximately

$$\int_{t_3}^{t_4} v^3 dt \sim \frac{(b^3 t)}{8760}\left[\frac{1}{4}\left(\frac{at}{b}\right)^3 + \left(\frac{at}{b}\right)^2 + \frac{3}{2}\left(\frac{at}{b}\right) + 1\right]\Bigg|_{t_3}^{t_4}$$

For a representative case where $V_R = 20$ mph, $t_1 = 876$ hours, $t_2 = 4820$ hours, $t_3 = 7000$ hours, and $\epsilon = 1.31$, then $t_4 - t_3 = 1628$ hours, and the ratio k_{eu} equals 1.51, that is, the DAWT provides 51 percent more power per year than the conventional WECS. For a lower value of $\epsilon = 1.0$, $t_4 - t_3 = 1100$ hours, and the ratio $k_{eu} = 1.37$, or the DAWT still provides 37 percent more annual power.

It has been observed that the actual power output of practical wind turbines with control systems, for winds at less than rated speed, is best described by a parabola, as $\int_{t_2}^{t_3} v^2 dt$, rather than by a cubic.

If we make the second term in the numerator of the equation for k_{eu} follow a parabolic relation, then the additional usable power of the DAWT is approximately

$$\int_{t_3}^{t_4} v^2 dt = \frac{b^2 t}{8760}\left[\frac{1}{3}\left(\frac{at}{b}\right)^2 + \left(\frac{at}{b}\right) + 1\right]\Bigg|_{t_3}^{t_4}$$

and for the example presented earlier, $k_{eu} = 1.05$ for the $\epsilon = 1.31$ case and $k_{eu} = 1.04$ for the $\epsilon = 1.00$ case. Thus, we may conclude that DAWT can improve the annual usable energy pattern between 5 and 50 percent, but that it depends very much on the control system characteristics for subrated power production and the spectral characteristics of the wind at the installation site.

DAWT/WECS COMPARISON

For our economic assessment of the DAWT we compare the capital cost per unit rated power of our present baseline design (e.g., augmentation ratio of 1.89, $L/D_2 = 0.5$, $A_4/A_2 = 2.78$, $\theta = 30°$) to a good WECS at cost levels associated with production quantities, on the order of 100 or more systems per year. This simplified evaluation is taken in lieu of a "cost of power to the consumer" approach which can become extremely complicated because of differing utilities accounting practices. A further advantage of our method is that it can be applied easily to any economic investigation already completed for WECS applications.

The details of our analysis consist of adding the average cost of the diffuser to the average cost of a wind turbine, for a particular wind turbine diameter, to find the average cost of the DAWT. We then have two options for evaluation:

1. Compare the DAWT to a WECS of equal turbine diameter
2. Compare the DAWT to a WECS of equal rated power

In the first case the average cost of the DAWT is divided by the augmentation ratio, r, to give the average cost for comparable rated power to the WECS. In the second comparison, the WECS turbine diameter is made greater than the DAWT diameter by $\sqrt{r}$, and the average cost of the WECS is determined for this larger turbine size. Although turbine diameters larger than about 65 meters are considered operationally unreliable at this time, we have extrapolated their costs from estimates for smaller diameters.

All costing information has been taken from the plots of Fig. 28. Results of the first cost comparison, for equal turbine

rotor size, are presented by Fig. 30. Using the Kaman rotor cost trends (Ref. 18), DAWTs are less expensive for all turbine sizes except a narrow size range of 40 to 45 meters diameter. With the latest GE cost trends (Refs. 19 and 20), the DAWTs are less

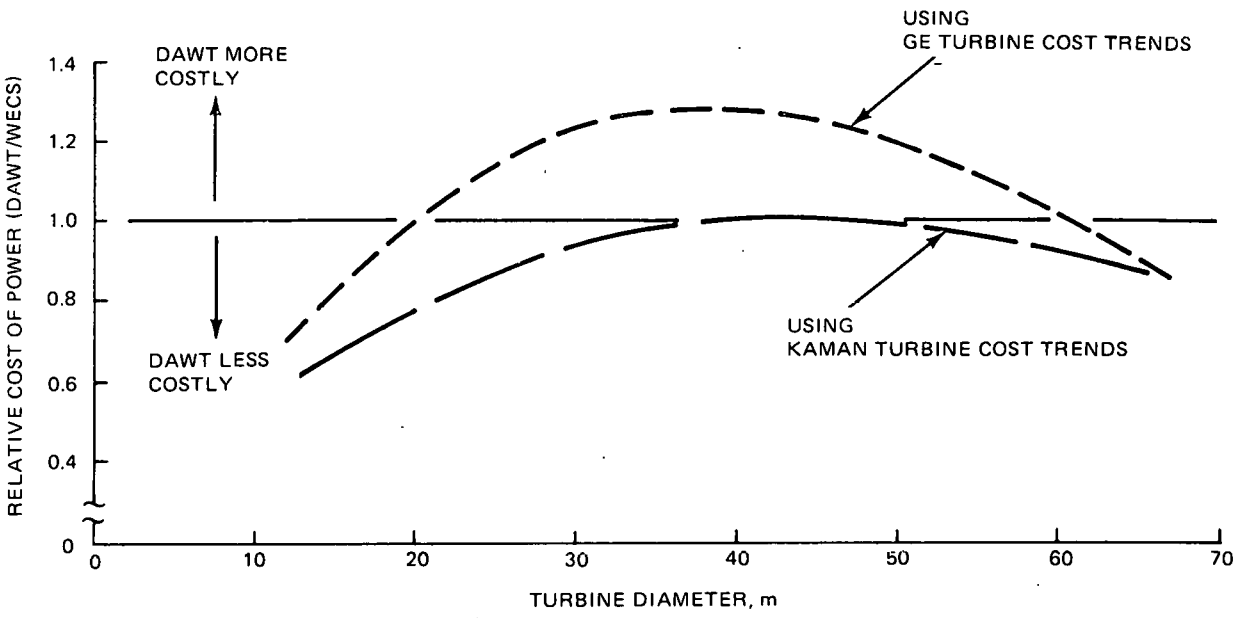

Figure 30 Cost Comparison of DAWT and Conventional WECS for Equal Rotor Size

costly for turbine diameters less than 20 meters or greater than 60 meters. In both situations, we have not taken advantage of the larger usable wind power factor, k_{eu}, of DAWTs compared to WECS. If this factor were to be introduced, it would significantly broaden the turbine size range in which DAWTs yield lower capital cost of power, when GE cost trends are assumed. The k_{eu} factor also would make DAWT significantly cheaper than WECS, especially if Kaman turbine cost estimates were to prove more realistic.

When a DAWT with an augmentation ratio of 1.89 is compared to a WECS of equal installed rated power, as shown by Fig. 31, the results are even more favorable toward the DAWT than for conditions

shown in Fig. 30. The excalation of average cost as turbine diameter increases works against the WECS, and makes DAWTs less costly for diameters greater than 45 meters, regarless of which authoritative estimate one applies towards the turbine. Particularly for the GE turbine cost estimates, DAWTs are more economical over the entire size range.

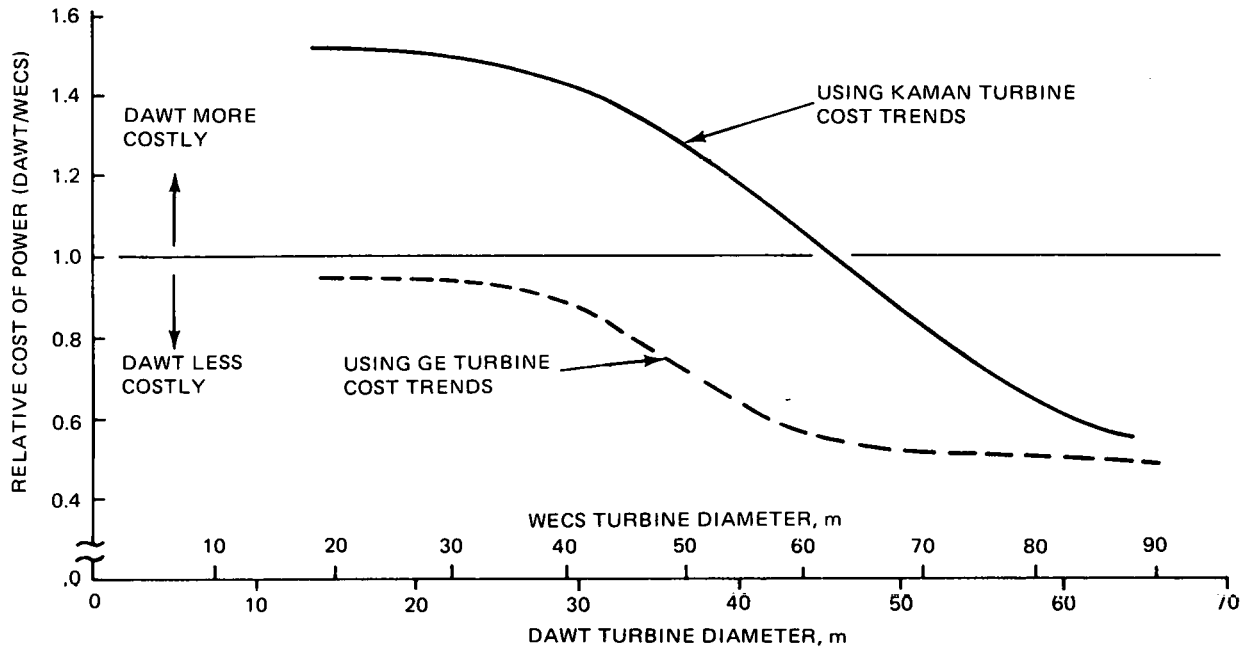

Figure 31 Cost Comparison of DAWT and Conventional WECS for Equal Rated Power

The economic consequences of Fig. 31 can be interpreted in two ways. The DAWT makes it possible to reduce capital costs for a desired power demand, or the DAWT can deliver much more power for the same investment capital as a WECS. In the first situation, the cost of electricity will be cheaper because interest carrying charges of investment are reduced; this favors the household consumer. In the latter situation, the economic growth prospects of the wind power user are enhanced and can result in a better future ability to pay the fixed carrying costs of the original installation; this is a favorable environment for industrial or commercial consumers.

In summary, these economic analyses, using modern turbine cost trends and our own diffuser-cost estimates for a boundary layer controlled design, show that DAWTs have lower cost per power than WECS for very large and small turbine diameter installations. The relative direct benefits of DAWT, especially in the intermediate size range, are somewhat obscured by the large uncertainty of current turbine cost estimates; the DAWT can be less costly to more expensive depending on whose authoritative judgement is used. The indirect benefits of DAWT, including a potentially greater annual usable wind energy factor, probably shades the economics in favor of the DAWT, regardless of turbine size or cost trends.

4. ANALYTICAL DEMONSTRATION OF TWO-STAGE CONSTANT SPEED ROTOR CONCEPTS

The objective of this part of the effort was to determine by analytical means whether a practical version of a stator-rotor system could be devised such that a constant speed rotor with fixed pitch could cover the usable wind range efficiently. We will refer to such designs as two stage wind turbines to distinguish them from rotor alone concepts. A two-stage wind turbine is a natural out growth of the use of a diffuser shroud, because of the streamlined struts that are necessary to support the hub within the shroud. By fitting each of the struts with controllable trailing edge flaps, or by rotating the entire strut, the inlet swirl to the rotor can be regulated to compensate for wind speed variations. This can eliminate the costs of rotor pitch variation, allow direct synchronous generation, and may show performance range advantages. The corresponding costs of controllable stators will depend on the number of stator blades required to provide sufficiently uniform rotor inflow. It should be a small cost for modest blade numbers, because the stators are static, and are loaded only by the slightly augmented wind velocity, not by the high relative wind of a rotor blade.

The initial work employed the concept of maintaining a constant rotor angle of attack for as wide a range of wind speeds as possible. This was accomplished by the scheme portrayed in Fig. 32. After some experimentation we realized that rotating the entire stator blade was always superior to use of trailing edge flap on the stator because the swirl induced by the TE flap produced a negative (i.e., counteracting) angle of attack on the fixed stator's leading edge. Even with this alteration, however, the peak efficiency range of the two-stage concept was narrower than we would like. By modifying the

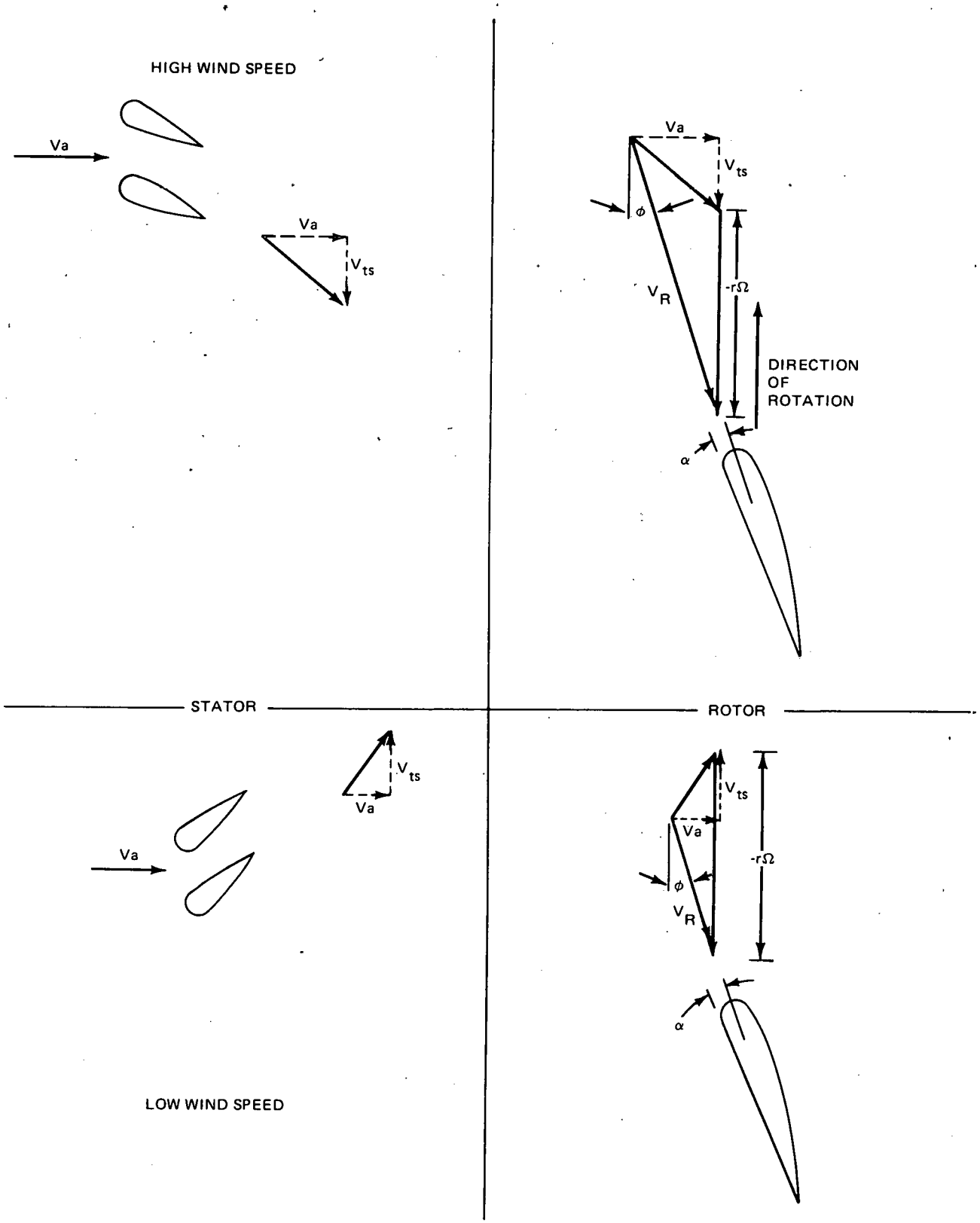

Figure 32 Velocity Triangle Diagrams of a Two-Stage Constant-Speed Wind Turbine

computer program to compute single-stage systems, a matched pair of stator and nonstator cases could be compared. This revealed for the first time that the off-design efficiency of the rotor alone was higher at all wind speeds than corresponding cases with the stator! Figure 33 shows such a comparison.

Why did the stator decrease efficiency even while maintaining the rotor at its most efficient flow angles and local disk loading? The governing equations are highly transcendental, so we have some difficulty showing the cause, but it seems evident that the adverse change in rotor relative velocity overcomes the favorable effect of maintaining the best rotor angle of attack. This effect is harmful only on the low wind speed side of the design point, because the high outputs at wind speeds much above the design point are not usable to the electrical system, so some means of reducing output must be employed. The pressure drop across the stator also plays a role, but it does not appear to be the main effect.

A stator based on a control law that seeks to maintain constant rotor angle of attack has been shown to be less effective than no stator at all. Is there then any purpose for a stator, when a strut system is needed anyway? There is one possible application: a stator preset for improving low wind speed performance by introducing a preswirl that increases (rather than decreases) relative velocity. This kind of stator would have an additional advantage of delaying stall of the rotor blades to higher wind speeds. One of the technological risk factors associated with any of the fixed pitch concepts used in different types of wind turbines is that unsteady effects associated with blade stall at high wind speeds may lead to unacceptable dynamic blade loadings. We have not investigated this type of fixed stator system as yet, because it requires another significant change in the computer program logic.

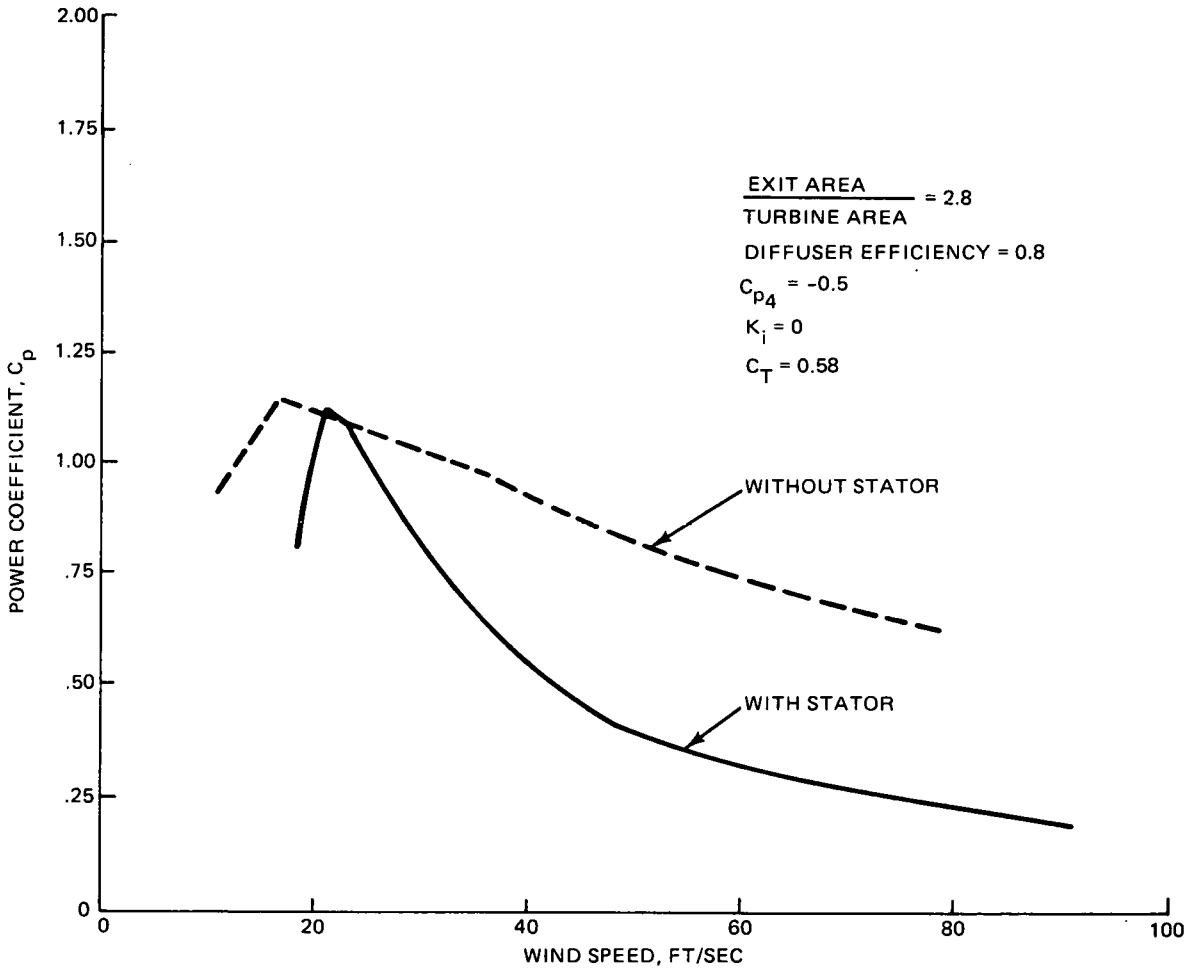

Figure 33 Computed Turbine Power Over the Wind Speed Range With and Without Stators

A small investigation of this possibility is planned for the next year's effort. We have reached the following conclusions:

1. Controllable stators are useful only as a possible means of inexpensive protection against overload at high wind speeds

2. A constant-speed, fixed-pitch rotor is practical without a controllable stator if the rotor dynamic design can withstand the oscillations of rotor blades operating fully stalled at high wind speeds

3. Because struts are needed anyway, there may be some value in introducing a constant preswirl to produce better performance at low wind speed with less rotor blade area, sacrificing performance at high wind speeds when the power available is greater than that which can be used by a controlled generating system

DESIGN TOOL

The Grumman computer program used for the analytical work of this task is called ROTOR. It is written in the Basic language, and is easily modified for the performance of special tasks. It is based on the Glauert vortex theory (Ref. 24) with suitable modifications to make that theory compatible with a two-stage turbine integrated into a diffuser shroud. The main modification to the original Glauert theory lies in the treatment of the axial interference factor, a. In the Glauert theory, each radial segment of the rotor determines its own axial interference independently of the other radial segments. In the ROTOR program the mean interference factor of the entire disk is applied uniformly to relate the disk velocity to the wind velocity through the performance of inlet, diffuser, and exit plane suction region. Ultimately design calculations will have to account for variations in axial velocity across the turbine radius, but since these will be strongly influenced by inlet design, the uniform case seems to be the most appropriate at this stage of development. The ROTOR program can be modified to consider radial variation in axial velocity at the turbine. The discussion of the previous section showed the significance of duct-induced velocity profiles.

Computations are performed from the turbine out to the wind. An assumed value of the axial velocity at the turbine is used to calculate turbine performance, then that performance is imposed on the duct performance to determine the external wind speed that corresponds to the assumed axial turbine velocity. This is a valuable time saver, because an iterative solution is avoided as long as a complete wind spectrum is covered. The stator and the duct each carry their own parameter set, and there is no closed form theory of the complete system to guide us. As a result, there will always be room for improvement in any designs we generate, but the ease of use and the speed of the ROTOR program and modern interactive time sharing computers enable us to find very good designs for particular purposes easily, and to survey the relative importance of different design parameters quickly. Several hundred design variations have already been calculated, and this experience is our main guide in selecting new designs.

It has been gratifying to note that the best design power coefficients calculated by ROTOR usually occur very close to the disk loading that is the theoretical optimum for the particular duct model being used, and the values of those power coefficients are of the order of 85 percent of the ideal power coefficient (i.e., a perfect turbine value). Some typical output data and stator angle sets are shown in Figs. 34 and 35.

ROTOR DESIGN

Full demonstration of the potential of the DAWT requires that the principles and performance be determined with working turbines, even though simulated turbines are very useful in developing diffuser configurations. To give the DAWT its proper assessment, it is necessary to know the turbine's efficiency at all operating

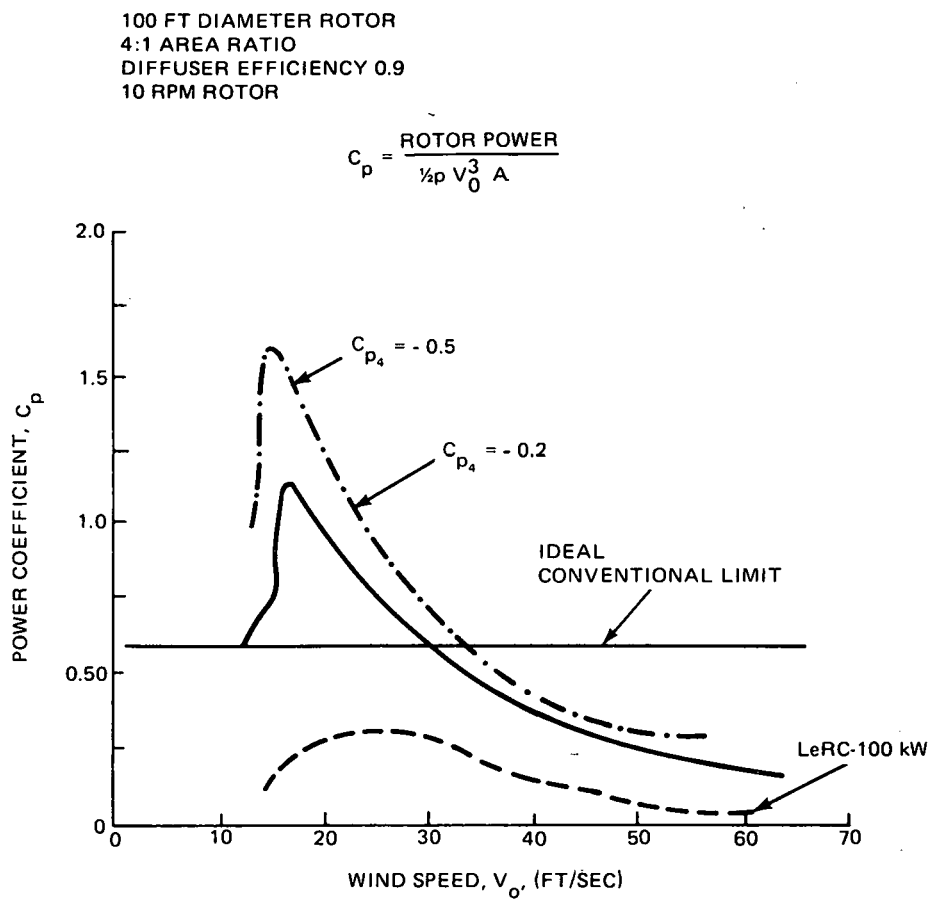

Figure 34 Diffuser Augmented Wind Turbine (DAWT) Performance

points. In order to avoid excessive expense for the design, construction, and calibration, a very simple, versatile and broad-ranged design is needed. We have adapted our rotor design program to evaluate various single-stage turbines in duct installations. The blades are of constant chord, constant section, and without twist, so extremely inexpensive rotors can be built to match desired characteristics shown first by analysis. Calibration in a duct of known flow and pressure drop will then provide the required turbine operating characteristics.

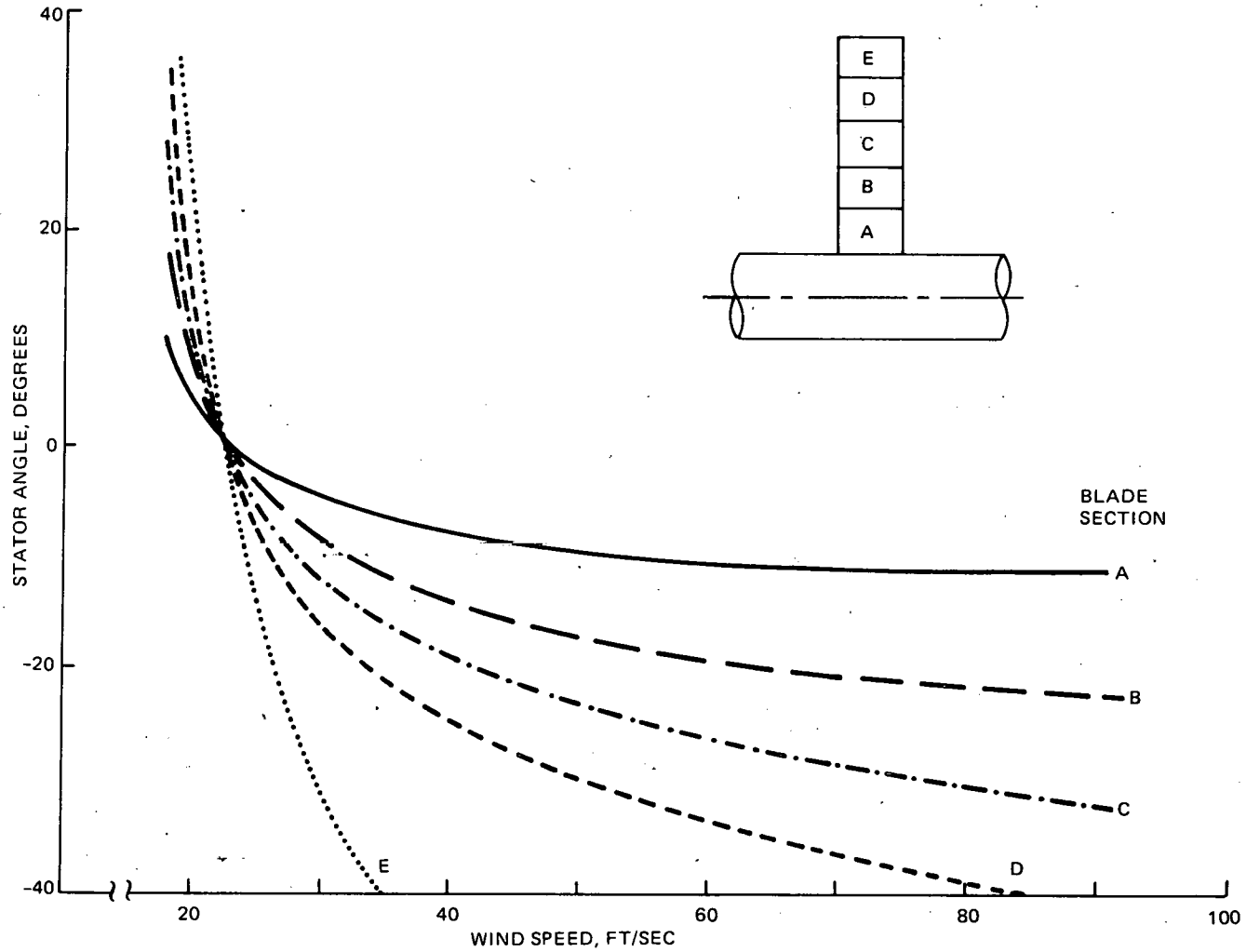

Figure 35 Typical Stator Flap Angle Program With Wind Speed

5. FUTURE WORK

The most important single factor in the DAWT development is to increase further its performance while minimizing the diffuser cost. Among the means to this end, the most important is probably a better understanding of the slot flow as it enters the high adverse pressure gradient of a 30° half-angle diffuser. This will allow more confident scaling to higher Reynolds number (i.e., larger sizes), and hopefully the maximum augmentation for each diffuser size. Another possibility is reducing structural cost by improved design features, and innovative concepts to relieve the high cost of meeting storm load survival criteria. The possibility exists also that some improvement may result from axial contouring of diffusers. The small scale results of the diffuser must be demonstrated at significantly greater scale, and in such a fashion that further scaling-up can be justified. The screen simulations of turbine output must be shown to be realizable (and improved upon) by a real turbine. Drag loads must be measured. The origin of the exit plane pressure reduction should be better explained. The baseline designs we have generated must be improved, both as the basis of construction of prototypes and as the basis for better cost estimates and economical evaluations.

6. REFERENCES

1. R. A. Oman and K. M. Foreman, "Cost-Effective Diffuser Augmentation of Wind Turbine Power Generation," Wind Workshop 2, F. R. Eldridge, ed., NSF-RAN-75-050, MTR 6970, The Mitre Corporation, September 1975.

2. O. Igra, "Shrouds for Aerogenerator," Report No. 2, Department of Mechanical Enginering, Ben Gurion University of the Negev, Beer Sheva, Israel, March 1975.

3. V. K. Shárán, "Characteristics of Flow Through Two Dimensional Screens and Perforated Plates," Journal of Sci. and Ind. Research, Vol. 34, No. 2, p. 82, February 1975.

4. "Pressure Drop in Ducts Across Round Wire Gauzes Normal to the Flow," No. 72009, Engineering Sciences Data Unit, London, England, June 1972.

5. A. Kogan and E. Nissim, "Shrouded Aerogenerator Design Study. I - Two Dimensional Shroud Performance," Bull. Res. Council of Israel, Vol. 1, pp. 67-88, 1962.

6. H. S. Fletcher, "Experimental Investigation of Lift, Drag, and Pitching Moment of Five Annular Airfoils," NACA TN4117, Washington, D.C., October 1957.

7. I. H. Abbott, A. E. von Doenhoff, and L. S. Stivers, Jr., "Summary of Airfoil Data," NACA Report No. 824, Washington, D.C., 1945.

8. S. H. Goradia and G. T. Calwell, "Analysis of High Lift Wing Systems," Aero. Quarterly, pp. 88-108, May 1975.

9. B. R. Williams, "An Exact Test Case for the Plane Potential Flow About Two Adjacent Lifting Aerofoils," ARC R&M3717, September 1971.

10. R. H. Liebeck and A. I. Ormsbee, "Optimization of Airfoils for Maximum Lift," J. Aircraft, Vol. 7, No. 5, pp. 409-415, September/October 1970.

11. I. H. Abbott and A. E. von Doenhoff, Theory of Wing Sections, Dover Publications, New York, 1959.

12. D. Küchemann and J. Weber, Aerodynamics of Propulsion, McGraw-Hill, New York, 1953.

13. I. S. Gibson, "Theoretical Studies of Tip Clearance and Radial Variation of Blade Loading on the Operation of Ducted Fans and Propellers," J. Mech. Eng. Sci., Vol. 16, No. 6, pp. 367-376, 1974.

14. W. F. Kappes, "Design Wind Loads for Building Wall Elements," in Wind Loads on Buildings and Structure, Bldg. Science Series 30, R. D. Marshall and H. C. S. Thom, eds., U.S. Department of Commerce, National Bureau of Standards, pp. 9-18, November 1970.

15. S. C. Hollister, "The Engineering Interpretation of Weather Bureau Records for Wind Loading on Structures," pp. 151-164, Ibid.

16. "Materials Leading Up in Price Despite Good Supply," Materials Engineering, Vol. 83, No. 1, pp. 69-74, January 1976; "The Economics of Materials," Materials Engineering, Vol. 8, No. 1, pp. 20-29, January 1975; Alcoa Price Data, Aluminum Sheet and Plate, Aluminum Company of America, Pittsburgh, Pennsylvania, July 7, 1975.

17. "Annual Survey of Manufactures, 1970-1971," U.S. Department of Commerce, Social and Economics Statistics Administration, Washington, D.C., 1971.

18. "Final Design Review. Conceptual Design, Parametric Analyses, and Preliminary Designs for Low Power (50-250 kW) and High Power (500-3000 kW) Wind Generator Systems," Contract No. NAS 3-19404, Kaman Aerospace Corporation, pp. 8-28, July 18, 1975.

19. "Final Presentation, Wind Turbine Generator Study," Contract No. NAS 3-19403, General Electric Space Division, Philadelphia, Pennsylvania, pp. 49-68, July 17, 1975.

20. R. L. Thomas, "Large Experimental Wind Turbines — Where We Are Now," NASA TMX-71890, March 29, 1976.

21. J. Johnston, Statistical Cost Analysis, McGraw-Hill, New York, 1960.

22. "Program for Conceptual Design, Parametric Analusis, and Preliminary Designs for Low Power (50-250 kW) and High Power (500-3000 kW) Wind Generator System," Contract No. NAS 3-19403, General Electric Space Division, Philadelphia, Pennsylvania, Document 75SDS4220, p. 37, April 22, 1975.

23. W. E. Heronenus, "The United States Energy Crisis: Some Proposed Gentle Solutions," paper presented to ASME, Springfield, Massachusetts, January 12, 1972.

24. H. Glauert, "Vortex Theory," Chapter VI in Aerodynamics Theory, Vol. IV, ed. by W. F. Durand, Dover Publications, New York, 1963.

U.S. GOVERNMENT PRINTING OFFICE: 1977-740-094/178